

Review

Progress of MOF-Derived Functional Materials Toward Industrialization in Solar Cells and Metal-Air Batteries

Mohamed Elhousseini Hilal ^{1,2,3} , Abdelkhalk Aboulouard ⁴, Abdul Rehman Akbar ^{1,2}, Hussein A. Younus ^{5,6} , Nesrin Horzum ⁷ and Francis Verpoort ^{1,2,8,9,*} 

¹ State Key Laboratory of Advanced Technology for Materials Synthesis and Processing, Wuhan University of Technology, Wuhan 430070, China; med.el.hilal@gmail.com (M.E.H.); ntuwtu@yahoo.com (A.R.A.)

² School of Materials Science and Engineering, Wuhan University of Technology, Wuhan 430070, China

³ Chemistry and Environment Department, Faculty of Science and Technology, Sultan Moulay Slimane University, Beni Mellal 23000, Morocco

⁴ Laboratory of Sustainable Development, Sultan Moulay Slimane University, Beni Mellal 23000, Morocco; a.aboulouard@gmail.com

⁵ Department of Chemistry, Faculty of Science, Fayoum University, Fayoum 63514, Egypt; hay00@fayoum.edu.eg

⁶ College of Materials Science and Engineering, Hunan University, Changsha 410082, China

⁷ Engineering Sciences Department, Izmir Katip Çelebi University, Izmir 35620, Turkey; nesrin.horzum.polat@ikc.edu.tr

⁸ Ghent University, Global Campus Songdo, 119 Songdomunhwa-Ro, Yeonsu-Gu, Incheon 406-840, Korea

⁹ National Research Tomsk Polytechnic University, Tomsk 634050, Russia

* Correspondence: francis.verpoort@ghent.ac.kr

Received: 17 July 2020; Accepted: 3 August 2020; Published: 7 August 2020



Abstract: The cutting-edge photovoltaic cells are an indispensable part of the ongoing progress of earth-friendly plans for daily life energy consumption. However, the continuous electrical demand that extends to the nighttime requires a prior deployment of efficient real-time storage systems. In this regard, metal-air batteries have presented themselves as the most suitable candidates for solar energy storage, combining extra lightweight with higher power outputs and promises of longer life cycles. Scientific research over non-precious functional catalysts has always been the milestone and still contributing significantly to exploring new advanced materials and moderating the cost of both complementary technologies. Metal-organic frameworks (MOFs)-derived functional materials have found their way to the application as storage and conversion materials, owing to their structural variety, porous advantages, as well as the tunability and high reactivity. In this review, we provide a detailed overview of the latest progress of MOF-based materials operating in metal-air batteries and photovoltaic cells.

Keywords: metal organic frameworks; catalysts; metal-air battery; solar cells; energy storage; energy

1. Introduction

The 21st-century daily life environment is increasingly conjoined with robotics, information technologies, and artificial intelligence. The promise of a more simplified future of assigning numerous delicate tasks to intelligent machines and expecting inferior error rates has paved the way for further developing existing technologies as well as the emergence of others, ranging from 5G network to assisted electric vehicles and smart homes [1–3]. Several similar high-technologies have already been implemented and progressively claiming a significant share of the market. Therefore, the demand for electrical energy will only keep spiking henceforth, with a 2.1% growth per year of the global

electricity demand, rising electricity share among other energy sources from 19% in 2018 to 24% in 2040 [4]. Sourcing and storing this form of energy is nowhere around the optimum yet, even though conventional batteries and specifically the lithium-ion (Li-ion) batteries have indeed revolutionized the history of storage devices and dominated the market of solar energy storage, because of their high energy density, relatively lightweight, and the long operation life. But some recorded unfortunate incidents have pinned doubts worldwide on the Li-ion batteries [5,6]. In addition, the ever-increasing need for more powerful storage devices leads the research laboratories to expand their investigation and explore more reliable alternatives with higher energy densities [7,8]. Metal-air batteries (MAB) present a far more ecological and secure candidate with much higher energy density than the best lithium battery conceived to date, almost approaching gasoline [9], and potentially serving as the future solar energy storage devices [8].

Both energy conversion and storage have always been complementary, coupling solar panels with MAB systems is a cutting edge technology used by pioneer energy companies [10]. The development of functional materials for both ends has been of cumulative progress. However, only a few operative materials have successfully made it out to the industrialization phase. Technically, for effective energy storage within MABs, oxygen evolution and reduction reactions (OER and ORR) are heavily involved, being the pivotal reactions, and at the same time, the bottleneck in the process, particularly with their high overpotentials. The industrially standard catalysts are always precious metals/metal oxides such as Pt, RuO₂, and IrO₂, by virtue of their excellent catalytic efficiency. Nevertheless, these rare, expensive materials are far from being multifunctional, for instance, Pt has poor OER activity while RuO₂ and IrO₂ are not good options for ORR, besides bigger stability problems and low surface area. However, metal-organic frameworks (MOFs)-derived materials are currently the most eye-catching for research, with great potential to serve the industry. In contrast to up-to-date industrially used precious metals, MOFs-derived catalysts come as robust and stable alternatives. Unlike most active materials, MOFs provide highly competitive controllability over the materials' functionalities, selectivity, mechanical, and chemical properties. This scarce and highly desirable tunability is derived from the wide available variety of ligands, metal centers, and synthesis methods. These chemical and structural features endow the MOF with superior specific surface area and excellent accessibility to a considerable number of different active sites. Therefore, MOFs have been among the most solicited materials to offer appropriately high catalytic performance, along with being both cheaper and scalable.

MOFs are formed from a metal cation center and an organic ligand, coordinated with defined crystallinity and porosity [11]. The synthesis controllability acquires them with a wide range of characteristics and crystalline porous structures with BET surface areas up to 7800 m²/g [12]. The absence of hidden volumes makes the MOFs significantly useful for volume-specific applications like adsorption, separations, purification purposes, and homogeneous catalysis [13]. However, because of the pristine MOFs' generally weak intrinsic conductivity and stability in harsh environments [14], they are mostly used as precursors to produce numerous functional derivatives, inheriting well-developed porosity and porous carbonaceous structures, as well as chemical constituents and morphology, which would eventually evolve into well dispersed and accessible active sites, which in turn lead to improved catalytic performance. MOFs have proven efficient not only for the storage but also for the conversion of light into electrical energy, combining two of the major potential solutions for nowadays energy crisis [15].

MOFs-based materials have been widely studied in solar cell applications because of their appealing physicochemical properties, great stability, large surface area, flexible structure, and low cost, serving as photoelectrode, counter electrode, and electrolyte for dye-sensitized solar cells (DSSCs) [16–18]. MOFs have also been extensively used in perovskite solar cells (PSCs) to improve crystallinity, morphology, and absorption in the visible region of perovskite as well as photovoltaic performance [19]. However, organic solar cells (OSCs)-based MOFs have not been extensively reported in the literature. The interesting results reported from the use of MOFs in PSCs and DSSCs would hopefully motivate the researchers to improve the efficiency of OSCs-based MOFs. Herein, we have

carefully selected and summarized the latest and milestones researches revealing recent progress of MOF-based materials, for both pivotal energy solutions [20].

2. MOF Based Functional Materials for Solar Cells

2.1. MOFs in Dye-Sensitized Solar Cells

Over the past few decades, many researchers have focused on dye-sensitized solar cells (DSSCs) because of their simple manufacturing and the ability to use inexpensive materials [21,22]. A standard DSSC is composed of: counter electrode, redox couple electrolyte, photoelectrode, as represented in Figure 1a [23]. TiO_2 has been commonly used as a semiconductor material that is frequently deposited on fluorine-doped tin oxide (FTO) as a thin film by using a doctor blade technique or screen printing. To enhance the cell's efficiency, the photoelectrode must have some criteria such as wide surface area and good transparency [24]. In a typical DSSC, the dye is a ruthenium complex adsorbed on the TiO_2 surface and captures sunlight photon [25,26]. During illumination, the dye gets excited from the ground state to the excited state and injects electrons into the conduction band of TiO_2 . The dye became oxidized and the electron gets diffused to the counter electrode via the external circuit. For the counter electrode, platinum is extensively used owing to inherent catalytic characteristics. Afterward, a liquid electrolyte, commonly consisting of redox iodide/triiodide (I^-/I_3^-), is used to regenerate electrons and relax the dye to its ground state [27]. Because of their good surface area, interlinked porosity, and structure flexibility, MOFs have been applied in DSSCs, which led to a noticeable improvement in cells' performance. MOFs application in DSSCs included its uses as a photoelectrode, counter electrode, and also as an electrolyte. The state-of-the-art of MOFs-based DSSCs are discussed in the following sections.

2.1.1. MOFs for DSSC Photoelectrode

A recent study was reported by He et al. where they utilized MOFs (ZIF-8 and UIO-66) and reduced graphene oxide (rGO) to modify the TiO_2 photoelectrode to enhance the photovoltaic performances of DSSCs [28]. In that composite, MOFs offer a high BET surface area for further dye adsorption, and rGO behaves as the collector of an electron to facilitate the transportation of electron from dye to the transparent conductive substrate. The short circuit density (J_{SC}) and conversion efficiency (η) of a simple TiO_2 photoelectrode are 11.6 mAcm^{-2} and 4.55% respectively, however, by using a modified photoelectrode with MOFs and rGO, improved J_{SC} and η were observed reaching 17.8 mAcm^{-2} , 7.33% and 18.6 mAcm^{-2} , 7.67% for ZIF-8-RGO/ TiO_2 and UIO-66-RGO/ TiO_2 , respectively. This enhancement is due to the increased dye adsorption on the photoelectrode.

ZIF-8 has also been reported as a blocking layer on the TiO_2 surface. Li et al. had demonstrated that the open-circuit voltage (V_{oc}) of DSSC could be improved when a thin layer of ZIF-8 (~2 nm) was deposited on TiO_2 . This could be attributed to the inhibited recombination of interfacial charge as a result of the addition of ZIF-8 as a shell [29]. The same approach has been reported by using *tris*(2,2'-bipyridine) cobalt (II)/(III) redox as an electrolyte; the DSSCs show an improvement in $J_{\text{SC}} = 11.89 \text{ mAcm}^{-2}$, $V_{\text{oc}} = 881 \text{ mV}$, $\eta = 7.75\%$ to $J_{\text{SC}} = 14.39 \text{ mAcm}^{-2}$, $V_{\text{oc}} = 897 \text{ mV}$, $\eta = 9.42\%$ (Figure 1b). This improvement is due to the enhanced electron lifetime and the amount of the dye adsorbed on TiO_2 , as well as the absence of the TiO_2 conduction band shift once ZIF-8 treatment was applied [30]. However, ZIF-8 was not exclusively used as a blocking layer for the photoelectrode but also as a composite material. The TiO_2 aerogel–MOF nanocomposite has been utilized in the photoelectrode, but the conversion efficiency was 2.34% [31]. To achieve good efficiency, the density of the electron trapping sites and the insulation properties must be optimized by decreasing the MOF content in the composite material [31]. MOFs were also used as sensitizers and co-sensitizers because of their hierarchically organized structures and appealing light-harvesting properties [16]. A series of zirconium (IV)-based MOF that integrate ruthenium (II) polypyridyl are grown as sensitizer on TiO_2 . Nevertheless, the cells efficiencies are lower than 1% [32].

2.1.2. MOFs for DSSC Counter Electrode

The counter electrode (CE) is an essential component of DSSCs which heavily affects the conversion efficiency of cells [33,34]. The CE has the role of collecting electrons from the external circuit and catalyzing the couple mediator in the electrolyte. The platinum is generally used as CE, as mentioned in the previous section. Because of its high cost, researchers have been utilizing alternative materials with low cost, good stability, and high catalytic characteristics [35–37]. Nowadays, MOFs were intensively studied for their appealing physicochemical properties which render them interesting materials for CE [38–40]. However, their employment as CE is quite limited because of the inherent mild conductivity, and the development of composite materials, including MOFs as well as conductive polymers, is typically needed to achieve the transport of charge in such application [41].

Liu et al. have synthesized $\text{MoS}_2@\text{Co}_3\text{S}_4$ composites-based material as CE via the hydrothermal route using ZIF-67 as a precursor. The conversion efficiency of 7.86% was obtained which is higher than that obtained with Pt CE (6.99%). This improvement was rationalized based on the good specific surface area and catalytic properties (Figure 1c) [42]. A transparent $\text{CoS}_{1.097}@\text{N}$ -doped carbon film derived from cobalt–metalloporphyrin MOF thin film was prepared on FTO as CE for bifacial DSSCs. The latter showed higher conversion efficiency (9.11% and 6.64% respectively) from the front and back illumination than Pt (8.04% and 5.87%) and with extended long-term stability [43]. Similarly, a transparent CE for bifacial DSSCs was also developed using *van der Waals* layer-by-layer (lbl) epitaxial growth protocol for preparing porphyrin-based MOF using (5,10,15,20)-tetra(4 carboxyphenyl) porphyrin ligand and zinc acetate (call Zn- TCPP)39. The conversion efficiencies of front and rear sides were reported to be 5.48% and 4.88%. This outstanding performance was attributed to the presence of single Pt atoms in porphyrin struts and to the SURMOF thin film high transparency [44]. Another excellent composite CE was prepared from ZIF-8 and polystyrene sulfonate-doped poly (3, 4-ethylene dioxythiophene) ZIF-8/PEDOT: PSS. The conversion efficiency obtained was as high as 7.02% which is roughly equal to the yield of Pt CE (7.24%), making ZIF-8/PEDOT: PSS as a good choice to replace the expensive Pt [18]. Even higher efficiency of 8.91% could be obtained when a new zirconium-based MOF-525 and sulfonated-poly(thiophene-3-[2-(2-methoxy ethoxy)-ethoxy]-2,5-diyl) (s-PT) composite film was deposited on a flexible carbon cloth substrate [17].

2.1.3. MOFs for DSSC Electrolyte

The electrolyte is an essential component and widely investigated, as described in the previous section. However, the deployment of MOFs for electrolytes for DSSCs has been scarcely reported, for instance, Bella et al. prepared a polymer composite comprising a Mg-based MOF via UV-driven free-radical process. The conversion efficiency reached 4.8% with exceptional long-term stability [45]. Sarwar et al. mixed an Al^{3+} -based MOF with a typical liquid electrolyte to form a gel electrolyte. The stability and photovoltaic performance of the gel electrolyte were significantly enhanced compared to liquid electrolyte alone [46].

In conclusion, relevant studies have been done during previous years in order to use MOFs in DSSCs. The main issue that faced photoelectrode and counter electrode based on MOFs to the overpass was the relatively low electrical conductivity. However, MOFs application as electrolyte shows their long-term stability and good photovoltaic performance. MOFs proved with great potentials but still need to be studied with the objective to enhance the overall performance of DSSCs.

2.2. MOFs in Perovskite Solar Cells

In recent years, perovskite solar cells (PSCs) have attracted the attention of researchers around the world because of their excellent photovoltaic performance. Continuous efforts have been paid to enhance the power conversion efficiency (PCE) throughout the past decades. From 2009 to 2019, the PCE was increased from 3.8% to 25.2%, which exceeded those obtained by traditional solar cells (CIGS and CdTe) [47,48]. Perovskite absorber, electrodes, hole, and electron transport layers are

generally the components of PSC. The three different standard architectures of PSCs are illustrated as seen in Figure 2 [49].

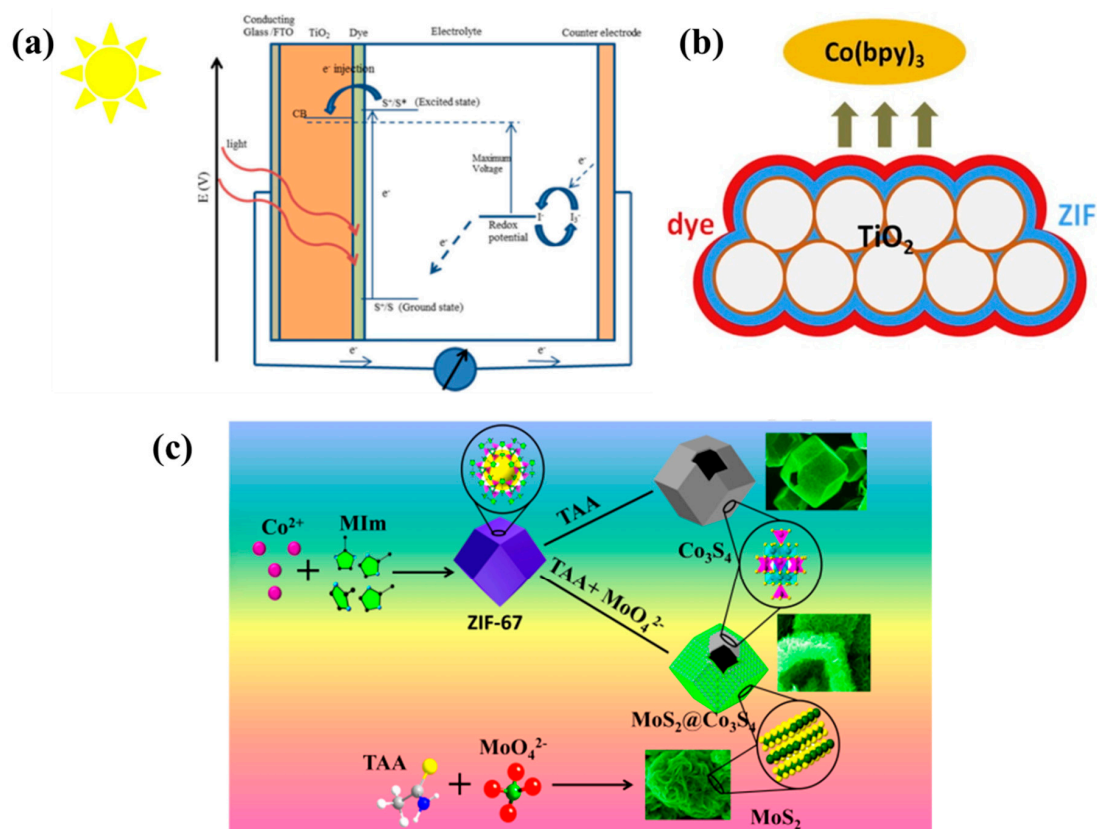


Figure 1. (a) A standard illustration of dye-sensitized solar cells (DSSC) [23]. (b) ZIFs as electron blocking layers for TiO_2 photoelectrode with tris(2,2'-bipyridine) cobalt (II)/(III) as electrolyte [30]. (c) The preparation schema of $MoS_2@Co_3S_4$ composites-based metal-organic frameworks (MOF) material ZIF-67 [42].

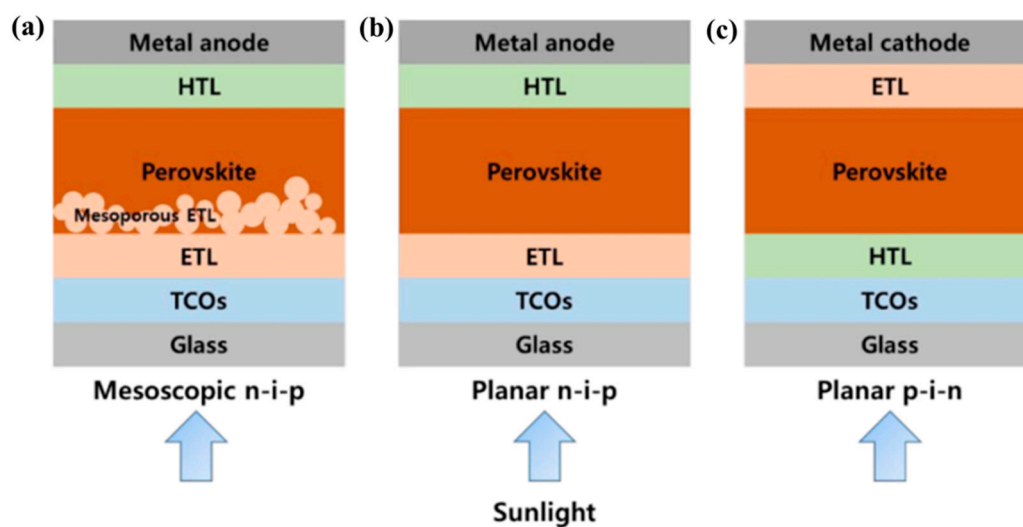


Figure 2. The standard architectures of perovskite solar cells (PSCs): (a) mesoporous n-i-p, (b) planar n-i-p, and (c) planar p-i-n [49].

In order to enhance the performance of PSCs, MOFs have been extensively studied by virtue of its numerous physicochemical features [50–53]. MOFs have been used in PSCs in three ways: 1—At the perovskite/charge transporting layer (CTL) interface; 2—as the electron transporting layers (ETL) or hole transporting layers (HTL) or incorporated within CTL; 3—within the interior of perovskite thin film. The recent progress of PSCs-based MOFs is reported in the next section.

2.2.1. MOFs in the Perovskite/CTL Interface

Vinogradov et al. are among pioneers to introduce MOF in PSCs. TiO₂-MIL-125 was prepared to replace pristine TiO₂, which behaved as ETL, as shown in Figure 3a. Furthermore, the PSC shows long stability in the ambient atmosphere and the PCE reached 6.4% [54]. Moreover, porous hierarchical (hier-TiO₂) nanostructure was prepared by sintering the MIL-125(Ti) MOFs. The hier-TiO₂ is deposited on a compact TiO₂ layer, making a dispersed scaffold and consecutively making quasi-mesoscopic PSCs, which enables the growth of large and stable perovskite grains (Figure 3b). Consequently, the stability and photovoltaic performance (PCE = 16.65%) were higher compared to TiO₂ nanoparticles as a scaffold (PCE = 11.38%) and TiO₂ compact-based planar PSC (6.07%) [52]. In the context of improving the sizes and the crystallinity of the perovskite as well as the photovoltaic performance, Shen et al. have incorporated ZIF-8 between mesoporous TiO₂ (mp-TiO₂) and perovskite interface serving as an additional scaffold to enable the development of crystals within perovskite. The optimum quantity of ZIF-8 would potentially crosslink adjacent perovskite grains, resulting in good growth of grains and satisfactory perovskite morphology, see Figure 3c. This incorporation proved effective for the elimination of carrier recombination and enhanced the extraction of charges. As a result, PCE of 16.99% could be attained which is superior to the cell with mp-TiO₂ (Figure 3d) [19]. A similar study where an inverted p–i–n PSCs were fabricated in order to enhance the efficiency of charge extraction and electrical contact between perovskite/NiO_x as an HTL interface by using two kinds of Zr-MOFs which are UiO-66 and MOF-808 (Figure 3e). The PCEs of modified PSCs are 16.55% and 17.01% for MOF-808 and UiO-66, respectively [55].

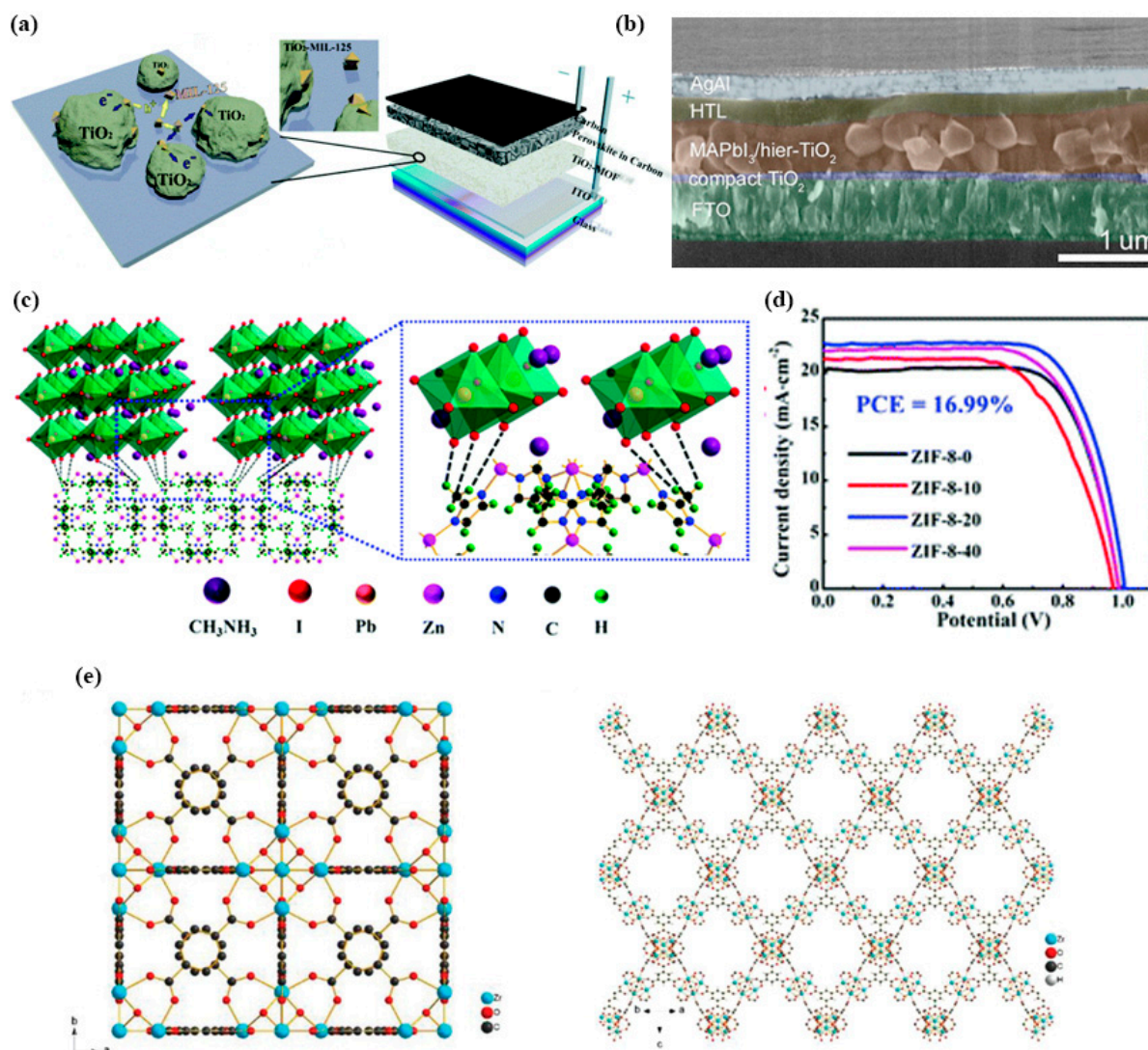


Figure 3. (a) Diagram structure of the photoactive composite and the depleted quasi-bulk heterojunction structure of TiO_2 -MIL-125 [54]. (b) Cross-sectional SEM of quasi-mesoscopic PSC using hier- TiO_2 deposited on compact TiO_2 layer [52]. (c) Schematic description of two adjacent grain structures linked by methyl groups of ZIF-8. (d) J-V curves of PSCs with ETLs containing ZIF-8-coated mp- TiO_2 for various times [19]. (e) The crystal structures of UiO-66 (left) and MOF-808 (right) [55].

2.2.2. MOFs for CTL or Incorporated with CTL

By using MOFs as CTL or incorporated with CTL, the efficiency of charge extraction is significantly enhanced, and the recombination of carriers is eliminated which improves the photovoltaic performance. Nanocrystalline Ti-based MOF (MIL-125) have been synthesized in order to engender ETL and substitute the standard TiO_2 ETL. Furthermore, Ti-based MOF (MIL-125) was incorporated with PCBM ([6,6]-phenyl- C_{61} -butyric acid) to increase conductivity and inhibits the close contact of perovskite and ITO (Figure 4a). Thereby, a good PCE was reached which is 18.94% [56]. By using the solvothermal method, Nguyen et al. prepared Co-doped TiO_2 with trimesic acid (H_3BTC) in the character of an organic framework to make the Co-doped Ti-MOF, see Figure 4b. The well-developed porous structure is obtained to use in PSC as an ETL. Therefore, an improved absorption in the visible region and a decrease in the hysteresis behavior has been observed, leading to an efficient charge extraction (PCE = 15.75%) [57]. Unprecedentedly, Yan and co-workers have employed ZnO instead of TiO_2 due to its higher electron mobility and structural heterogeneity which make it much more appealing.

The as-synthesized ZIF-8-derived ZnO was used as ETL; the latter exhibits a particular morphology, great contact area, and large internal pores which leads to an intriguingly high PCE = 18.1% [58].

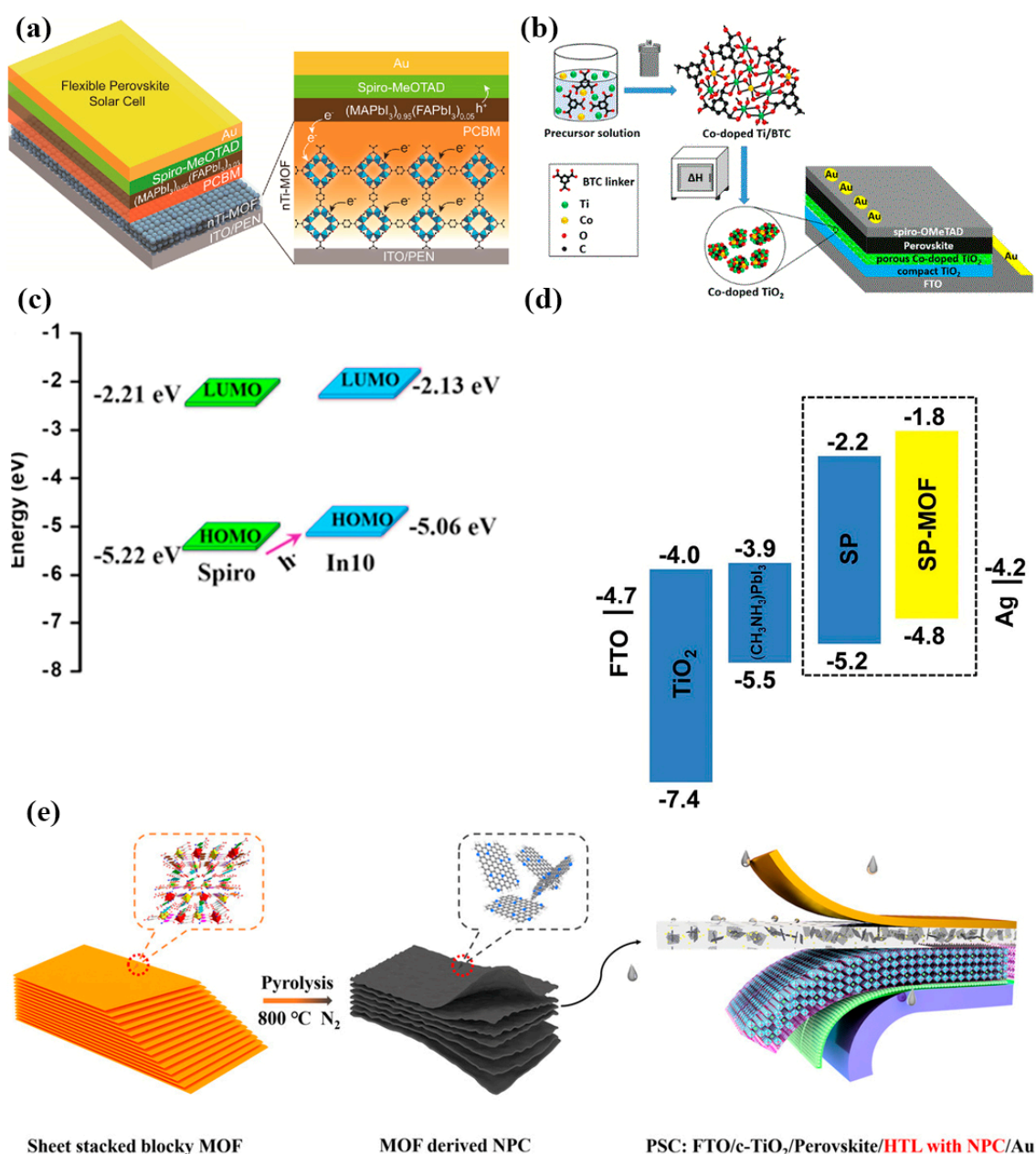


Figure 4. (a) Energy levels of Spiro-OMeTAD and In10, (b) J–V curves of HTM, and HTM/In10 with different amounts of In10 [59]. (c) The reflection spectra of Spiro-OMeTAD (SP) and SP-MOF samples, (d) energy levels of PSC with Spiro-OMeTAD (SP) and SP-MOF as HTL [60]. (e) The scheme of direct MOF crystals pyrolysis into graphitic NPC as HTL [61].

MOFs can also be used in HTL. Li et al. introduced a MOF, specifically, $[\text{In}_{0.5}\text{K}(\text{3-qlc})\text{Cl}_{1.5}(\text{H}_2\text{O})_{0.5}]_{2n}$ (In10) into (2,2',7,7'-tetrakis(N,N'-di-p-methoxyphenylamine)-9,9'-spirobifluorene) (Spiro-OMeTAD)) resulting in enhanced conductivity of HTL. As illustrated in Figure 4c, there is no large energy barrier between the In10 and Spiro-OMeTAD HOMOs. This leads to integrate In10 into Spiro-OMeTAD and could be advantageous for hole transfer at the perovskite-HTL interface, which in turn led to PCE of 17%. This achievement is attributed to the positive role of In10 in promoting perovskite sunlight absorption and avoiding penetration of moisture [59]. Huang et al. synthesized lead-based MOF ($\text{Pb}_2(1,3,5\text{-HBTC})_2(\text{H}_2\text{O})_4$, (Pb-MOF) which is doped into Spiro-OMeTAD material. In contrast to the

simple Spiro-OMeTAD layer, the composite layer exhibits a smoother surface, great hydrophobicity, and electrical interfaces. The energy levels of Spiro-OMeTAD-MOF HTL in the PSC are more suitable to the nearby layers of perovskite and Ag (Figure 4d). Consequently, the PCE of the PSC-based Spiro-OMeTAD-MOF HTL is 13.17% which is higher than that of the pure Spiro-OMeTAD HTL [60]. A planar heterojunction PSC was fabricated by Zhou et al. by implementing (MOF)-derived N-rich porous carbon (NPC) into HTL. This latter is composed of bidopants bis(trifluoromethane) sulfonimide lithium salt (Li-TFSI) and 4-tertbutylpyridine (t-BP) which are doped on Spiro-OMeTAD. This structure is achieved from the direct pyrolysis of a 2D In-based MOF In-Aipa, $[\text{In}_2(\text{Hipa-NH}_2)_2(\text{ipa-NH}_2)_2] \cdot 5\text{H}_2\text{O}$ ($\text{H}_2\text{ipa-NH}_2 = 5\text{-aminoisophthalic acid}$), as illustrated in Figure 4e. The implementation of NPC decreases lithium salt aggregation and HTL defect formation, enhancing film quality for efficient hole extraction and redistribution. The fabricated cell has a PCE = 18.51% [61].

2.2.3. MOFs into Perovskite Thin Film

The first study about introducing MOF into perovskite thin film was reported by Chang et al. A simple strategy to enhance the crystallinity of the perovskite thin film was achieved by introducing MOF-525 as additives in the precursor solution. This integration serves as a typical scaffold to permit perovskite to be crystallized inside. Therefore, the scaffold offers an orderly structure of perovskite crystallites during the initial crystallization stage. The PCE of the PCS with the enhanced morphology and crystallinity is 12% [62]. Lee et al. combined two types of Zr-based MOFs (UiO-66 and MOF-808) into the perovskite precursor. The resulting PSCs showed higher PCE = 18.01% and 17.81%, respectively. In addition, the long-term stability of PSCs-based UiO-66 and MOF-808 are higher than the pristine cell [55]. Very recently, Zhou et al. have incorporated In(III)-based MOF, namely, $[\text{In}_{12}\text{O}(\text{OH})_{16}(\text{H}_2\text{O})_5(\text{btc})_6]_n$ (In-BTC) with perovskite to form heterojunction light-harvesting layer to enhance light absorption, crystallinity, morphology, and stability of the perovskite thin film. The PCE of the resultant heterojunction perovskite/In-BTC is $19.63 \pm 1.24\%$ [63].

In summary, MOFs have been used in PSCs to eliminate carrier recombination, enhance the efficiency of charge extraction, improve the absorption in the visible region, increase the long-term stability, and decrease the hysteresis behavior. Moreover, MOFs can enhance the morphology and crystallinity of perovskite thin film. Future works may open new roads to find other functions or advantages of MOFs in PSCs.

2.3. MOFs in Organic Solar Cells

Organic solar cells (OSCs) are made from small molecules, polymers or both by easy and cost-effective techniques, like spin coating, printing, and spray deposition. Thus, OSCs are inexpensive and simple to manufacture. The ITO is the most frequently used as transparent conducting oxide (TCO), obviously having a double function: the role of the anode in addition to allowing light to penetrate into the active layer. Then, PEDOT:PSS (poly(3,4-ethylenedioxythiophene) polystyrene sulfonate) is deposited as an electron-blocking layer and it also enhances the movement of holes to the anode. In the bulk-heterojunction (BHJ) structure, the electron-blocking hole-transport layer (HTL) is important in contrast with the bilayer structure. The absence of HTL in BHJ results in low photovoltaic performance because the hole and electrons both move to the same electrode. Furthermore, the active layer contains organic materials that are acceptor and donor used as a layer to form bilayer cell or mixed to form BHJ cell. Carbon nanotubes (CNTs) have recently been utilized as accepters rather than organic acceptors to establish an active layer of the nanocomposite. The final component is the cathode that is mostly copper or aluminum (Figure 5a) [64].

As already discussed in the previous sections, the use of MOFs in DSSCs and PSCs has been well examined; however, MOFs application in OSCs have not been much investigated up to now. Xing et al. have recently succeeded in synthesizing a novel 2D tellurophene-based MOFs by using cadmium nitrate and tellurophene-2,5-dicarboxylate. Afterward, polyethylenimine ethoxylate (PEIE) was utilized to exfoliate the 2D tellurophene-based MOFs to make single- and multi-layer MOF

nanosheets and used them as an electron extraction layer (EEL) for OSCs. When the hybrid MOF-PEIE was utilized as EEL it showed 15% improvement on photovoltaic performance compared to the PEIE layer owing to the recombination of the suppressed charge and enhancement of the conductivity (Figure 5b) [20]. This achievement opens new roads for MOF to be incorporated into OSCs.

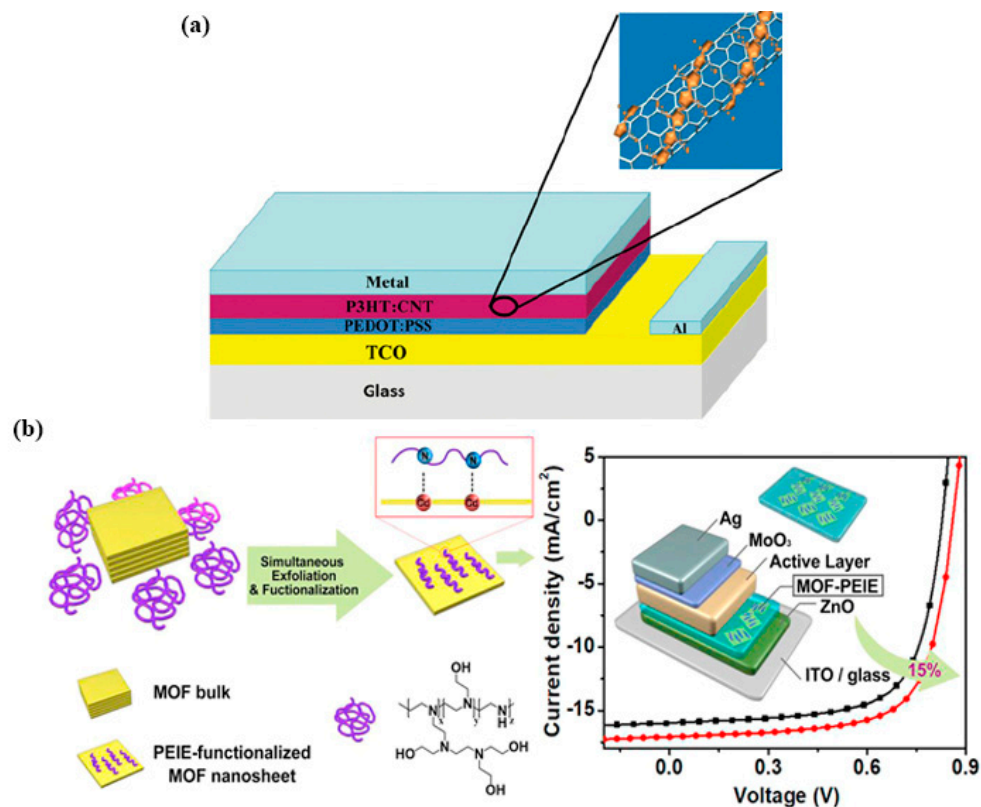


Figure 5. Graphical diagram of (a) standard organic basic cell using carbon nanotubes as an acceptor in the active layer [64]. (b) Preparation diagram of MOF-PEIE and its application in organic solar cells (OSC) [20].

3. MOF Based Functional Catalysts for Metal-Air Batteries

Metal-air batteries (MAB) are generally composed of a metal anode, mostly Li, Zn, Al, Na ... then a solid or liquid electrolyte and an air cathode, this applies on: (i) the mechanically rechargeable MAB, where the metal plate and sometimes also the electrolyte are changed after consumption during discharge. (ii) The solid-state MAB where the electrolyte is in the solid phase, generally PVA-based gel-polymer for Zn-air batteries. (iii) The electrically rechargeable MAB, that features an open battery model where the cathode is a breathing carbon-based or metallic porous foil, called gas diffusion layer (GDL), supporting the indispensable bifunctional electrocatalyst [65,66].

As a matter of fact, the performance of the MAB is systematically related to the quality of all three components. Nevertheless, the air-cathode electrocatalysts have attracted most of the attention, and that is due to hosting oxygen evolution and oxygen reduction reactions (OER and ORR), being the primordial reactions for the functioning of MAB. Therefore, the engineering of novel non-precious functional materials to accelerate the sluggish OER and ORR is of great importance. Over the past few years, MOFs stands out as a very promising and cost-effective candidate for air cathode materials, besides being a powerful tool to understand the functioning and the process during charging and discharging of the metal-air batteries, owing to their tunability and design controllability [67–69]. MOF-derived graphitized carbon facilitates the electrons transfers and proves strongly obstructing alteration during the charge-discharge process [70–72]. Besides that, the high surface area and the 3D porous structure not only multiply active sites and increase their accessibility but also favor the

penetration of electrolyte and oxygen to successfully form the desired three-phase state [73]. Moreover, MOF-derived carbon materials could provide highly sought electrocatalytic bifunctionality, either by high dispersion of a single kind of catalytic active sites that could catalyze both reactions i.e., OER and ORR, or by containing bimetallic/heteroatoms-based active sites or even host dual phases to approach the reactions in different mechanisms within the same catalyst [74]. This provides a profitable opportunity to synthesize and design a multitude of highly efficient bifunctional catalysts. Therefore, you will find hereafter the recently reported progress of MOF-based electrocatalysts specifically serving lithium-air batteries, zinc-air batteries, and others that are judged the most likely to be industrialized in the few coming years.

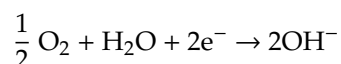
3.1. Zn-Air Batteries

The first Zn-air batteries have appeared in the early 19th century; however, their massive bulky nature with low current capacity did not gain them much appliance [75]. In 1997, rechargeable Zn-air batteries returned to the surface by Miro Zorič [75]. Henceforth, many preliminary studies have been carried out to develop this technology as nowadays the most affordable storage option for an energy density reaching up to 1300 Wh.kg [76]. Extensive investigations on the anode materials and electrolytes have had a great impact on the industrialization of Zn-air batteries, overcoming the main challenges regarding dendrites, electrolytes leaks, and dryness. However, the bifunctional catalysts have been holding most of the attention because of the key role of promoting vital reversible oxygen reactions. Actually, the discharge mechanism of rechargeable Zn-air battery in aqueous alkaline media starts by the oxidation of Zn anode liberating couple electrons used for oxygen reduction reaction (ORR), the overpotential of this reaction is lowered by the electrocatalyst on the cathode; meanwhile, ZnO is formed by the reaction of the byproduct zincate ions to hydroxide and water [77]. During the charging process, the reversible process takes place and Zn cations get reduced and restore the Zn anode content.

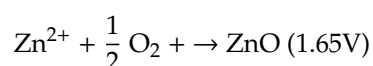
Anode:



Cathode:



Overall reaction:



In laboratories, developing air-cathode bifunctional catalysts have taken serious steps forward recently using multiple technics and elemental combinations, but always, in order to reach a power density above 200 mW/cm² and a high specific capacity over 800 mAh/g, coupled with significantly long life cycles, the bifunctional electrocatalyst should be carefully designed to be effective for both oxygen reactions and show excellent stability in such corrosive environment. Therefore, we will discuss hereby the most efficient and recent technics yielding state-of-the-art bifunctional catalysts for ZAB.

3.1.1. MOF-Derived Single-Atom Catalysts

The single-atom catalysts have sparked important interest in their high electrocatalytic efficiency; this feature is directly inherited from the high atom utilization compared to other kinds of catalysts. The well-dispersed active metal atoms act very efficiently in hosting oxygen reactions for their high surface free energy [78–81]. Highly active FeN₄ sites have been anchored on 3D hierarchical carbon, derived from the pyrolysis of ferrocene-encapsulated ZIF-8 precursor. The resulting 3D hierarchically ordered microporous-mesoporous-macroporous nitrogen-doped carbon 3DOM Fe-N-C-900 has successfully avoided common flaws of MOF-derived Fe-C-N active sites being contained in microspores and often inactive (Figure 6a) [82]. 3DOM Fe-N-C-900 has catalyzed ORR for ZAB and achieved a remarkably high power density of 235mW/cm² and a high specific capacity of 768.3 mAh/g_{Zn}.

The hierarchical carbon has exposed and stabilized single active atoms against migration by reducing their kinetic barrier of mass transport that usually causes agglomeration. The methanol tolerance test confirmed the high stability of the active sites with 90.2% retention after 20 h continuous operation in contrast to 38.8% loss for Pt/C catalyst under the same conditions [82].

Besides, iron and cobalt-based MOFs have always been attractive for ZAB air cathode catalysis, because of the fact that reduced cobalt atoms get embedded in the N doped carbon matrix deriving from MOF at high temperatures [83]. The carbonization of heterostructured Co/Zn-ZIF@ZIF-67 has produced an interesting core-shell structure of single $\text{Co-N}_x\text{C}_{4-x}$ active sites enveloped by highly graphitized porous carbon, as shown in Figure 6b. The number of N and C around cobalt single atoms was tuned by pyrolysis temperature. At 900 °C, $\text{Co-N}_3\text{C}_1$ @GC single-atom catalyst is reported to dramatically enhance the mass transport and the electron transfer, which endorse the catalyst-based ZAB, delivering a peak power density equal to 255 mW/cm^2 and outperforming Pt/C benchmark (Figure 6c). It is to note that DFT calculations revealed that CoN_3C_1 is the best electrocatalyst, as compared to $\text{Co-N}_2\text{C}_2$ and Co-N_4 , to exhibit near-Fermi electronic states, which promotes the electronic hybridization with O_2 and the step of protonation of adsorbed O_2^* [84].

Wagh et al. have designed single-atom coordinated hollow nano-spheroids of nitrogen-deficient carbon nitride by a two-step process, co-precipitation followed by annealing the metal-carbonitride complex to get supramolecular assemblies of metal single-atom catalysts. The absence of metal nanoparticle or clusters has confirmed the dispersion and confinement of single metal atoms by high magnification TEM. After testing the partially filled anti-bonding state of different metals (Cu, Fe, and Co), Cu turned out to be with the most suitable binding strength of intermediates with a d-band center value of -2.46 eV the closest to that of Pt (-2.67 eV), implying remarkable oxygen reactions catalysis in Figure 6d. The intriguing exposure of Cu single atoms offered by the highly porous crumpled nano-spheroids has attributed CuSA@HNCN_x -based ZAB a high power density of 212 mW/cm^2 at 360 mA/cm^2 , with a relatively high open-circuit voltage (1.51 V) and specific capacity of 806 mAh/g_{Zn} as shown in Figure 7a. The nitrogen-stabilized Cu single-atom catalyst has proven stable cycling of over 1800 cycles (of 10 min each) @ 10 mA/cm^2 [85].

3.1.2. MOF-Derived Bimetallic Catalysts

A successful synthesis of MOF-derived 3D carbon matrix composed of transition metal alloys has been a prominent way to acquire high-efficient and durable catalysts for ZAB's air cathode oxygen reactions. One very recent research has fabricated FeNi alloy nanoparticles inlaid by sacrificial ZIF-8 templating on nitrogen-doped carbon electrospun nanofibers. Tafel plots affirmed the important coupling of the bimetallic electrocatalyst by evaluating the slopes; FeNi/N-CPCF-950 has the smallest slope value of 67 mV/dec , whereas the rest of the samples with either iron or nickel-metal centers were much higher. Beside FeNi synergistic effects, the abundance of FeNi NPs in the hierarchically porous structures and the self-standing carbon structure owing to the electrospun microfibers enabled FeNi/NCPCF-950 bifunctional catalyst to endow ZAB with a fairly high energy efficiency of 61.5%, with small charge-discharge voltage gap of 0.764 V, and more importantly, an outstanding 20 min charge/discharge cycles based astonishingly long stability performance of 640 h at 10 mA/cm^2 under ambient conditions (Figure 7b) [86]. In order to investigate the synergistic effect of multiple metal centers, two trimetallic catalysts for OER and ORR have been produced by Agarwal et al. starting from ZIF-8 supported on tellurium-derived porous carbon nanotubes and ZIF-67, and further doping iron species. The resultant mixed-metals composites CoFeZn@pCNT (at porous carbon nanotubes) and CoNiFe-S@GC (at Graphitized carbon) derived from ZIF-67, were respectively used for ORR and OER of the ZAB air cathode. Showing a competitive round-trip overpotential of the cell is ca. 0.6 V [87]. Matériaux and co-workers have managed to synthesize a novel design of multiple transition metal bifunctional electrocatalysts $\text{Fe}_2\text{Ni}_2\text{N/Co@NCNT}$ starting with the three metal cations Ni^{2+} , Fe^{2+} , and Co^{2+} . This design has developed highly dispersed trimetallic nanocrystals strongly coupled to a

porous N-doped carbon, delivering an ultra-long life rechargeable ZAB exceeding 850 h at 5 mA/cm² with an outstanding 83 mV charge-discharge gap at 20 mA/cm² [88].

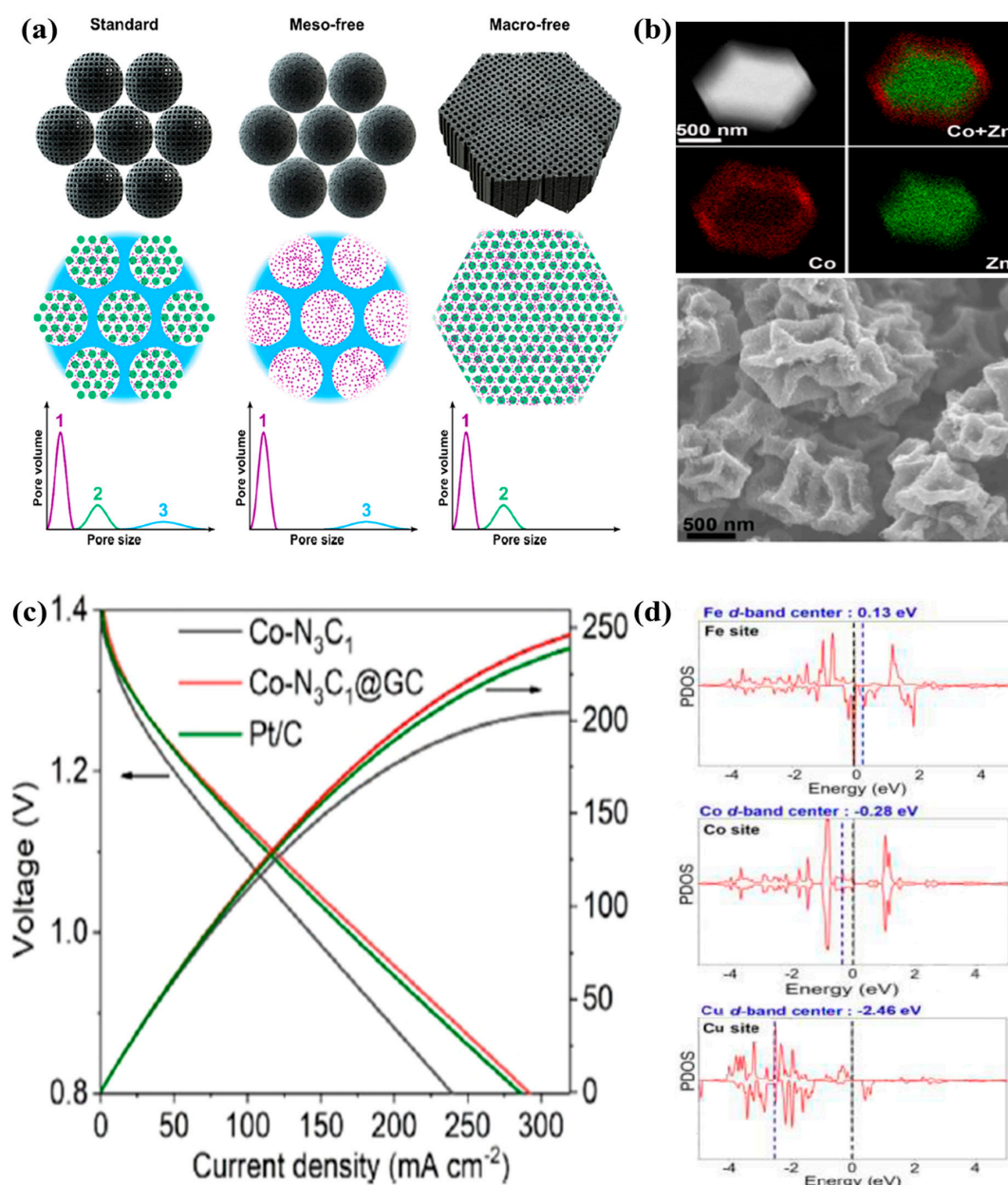


Figure 6. (a) The scheme and porous structures of the three model catalysts [82]. (b) The STEM-EDS elemental maps and SEM images of Co/Zn-ZIF@ZIF-67 [84]. (c) The polarization curve and power density plot of the battery [84]. (d) The partial density of states (PDOS) of Fe, Co, and Cu in FeSA@HNCN_x, CoSA@HNCN_x, and CuSA@HNCN_x, respectively [85].

3.1.3. Heteroatoms Doped MOF-Derived Carbon Catalysts

Recently, heteroatoms-doped carbon materials have attracted great attention by being environmentally benign and easily inserted into specific locations in the carbon matrix, and still exhibiting the ultrahigh active and atomically dispersion of metal atom—non-metal atom—carbon active sites, resulting in substantial decreases in ORR and OER overpotentials and efficient Zn-air battery performance [89]. The interest in this kind of doping stems from two mechanisms: the first whereby the high dispersion on the surface promotes the catalytic reaction, and the second where

doped heteroatoms act as very reactive sites toward adsorption of water or hydroxide molecules to form oxygen gas [87].

For instance, N-doped carbons have been the most investigated materials for Zn-air batteries, owing to inherent nitrogen electronegativity and the enhanced π bonding that improves electron-donor acceptor properties [90], therefore electrocatalytic activity, high durability, and cost-effectiveness [91]. A recently reported dual-doped metal-free air cathode catalyst has shown impressive results open circuit potential of 1.48V, a power density of 208 mW/cm² and an energy density of over 870 Wh/kg [92]. This P-, N-doped carbon has proven to particularly promoting the adsorption of oxygen via the vacant 3d orbitals of P/N by valence electrons, as in Figure 7c [93]. P, N co-doping induced defects that led to highly localized states nearby Fermi level [94,95] improved the physicochemical properties of the carbon framework that boosted the electrocatalytic activity (Figure 7c) [96,97].

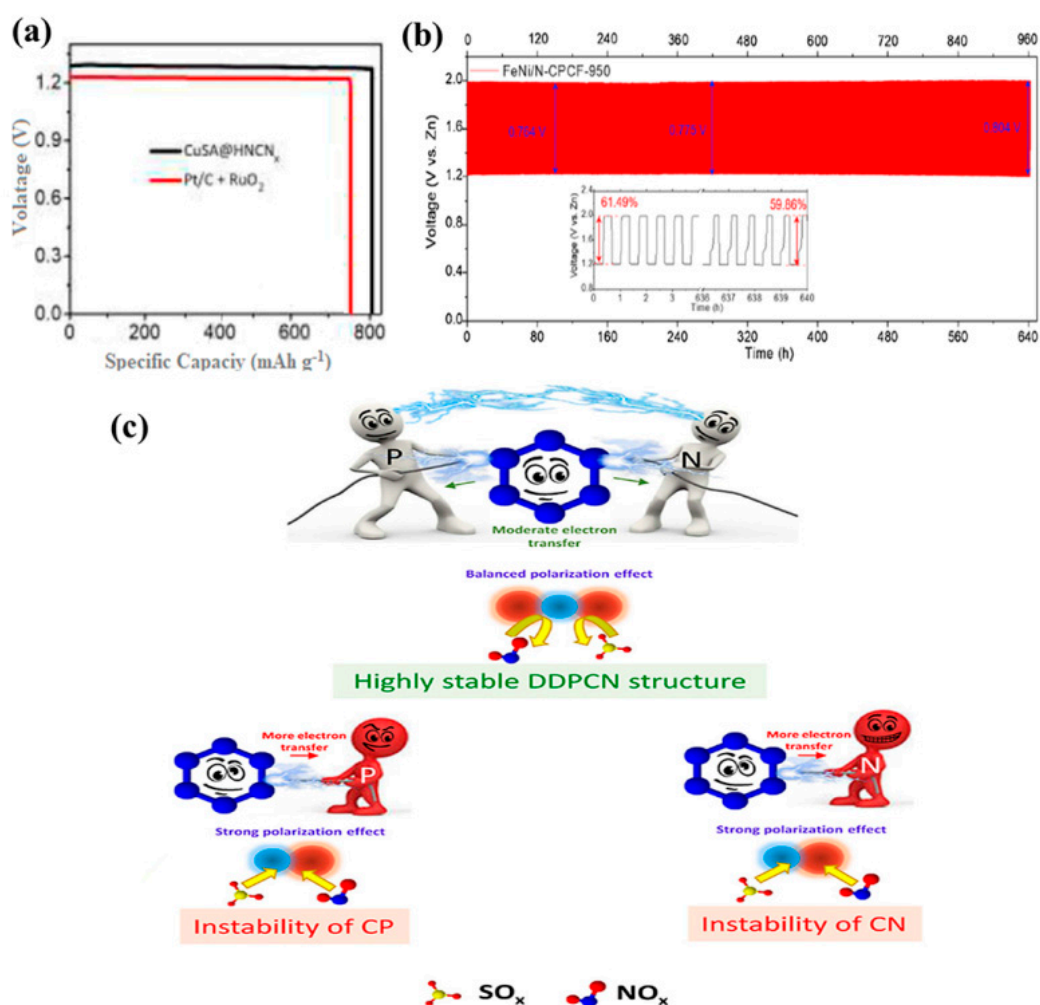


Figure 7. (a) Specific capacities of for CuSA@HNCN_x and Pt/C+RuO₂ cathodes [85]. (b) The 640 h galvanostatic cycling stability of Zn-air battery with FeNi/N-CPCF-950 air cathode catalyst (at 10 mA cm⁻²) [86]. (c) The structural resistance of P, N dual-doped porous carbon nanospheres (DDPCN), nitrogen-doped carbon (CN), and phosphorous-doped carbon (CP) for the incoming small molecules NO_x and SO_x [92].

3.2. Li-Air Batteries

The lithium air/lithium–oxygen battery has wide-reaching consideration as the forthcoming energy source, owing to its very high theoretical energy density (~3500 Wh/kg) [98]. Agraham et al. have reported the first lithium-air battery with a structure of Li |organic electrolyte| air in 1996 followed

by a series of work by other researchers [99]. Lithium-oxygen (Li–O₂) batteries got consideration as a prominent and efficient candidate in energy storage owing to their high potential energy densities and the plentiful and low-cost O₂ supply [100]. But for lithium-air battery, the discharge product Li₂O₂ is not soluble in an organic electrolyte and gradually chokes the porous air electrode [101]. Several technical encounters made it far behind the practical usage. The lethargic kinetic reactions at the air-electrode provoke serious issues, such as, the small round-trip efficiency and reduced rate capability. Though several efforts have been practiced minimizing the polarization, and certain progress has been accomplished, the cycle life is still relatively inadequate because of the deterioration of the electrolyte and anode [98]. Specifically, the huge overpotential needed for the Li₂O₂ recharge encouraged researchers to investigate effective Li₂O₂ charging catalysts. Bi-functional catalysts such as precious metals-based (Pt-based, Ru-based) or metallic oxides (MnO_x, CrO_x, and CoO_x) revealed to be effective in decreasing the overpotential of the OER [102].

The reaction mechanisms during discharge ORR and charge OER are the fundamentals for additional development while the overall electrochemical reaction of Li–O₂ batteries in non-aqueous is as follows in (Reaction (1)):



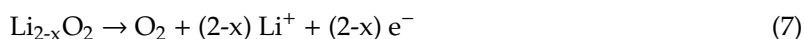
The discharge ORR mechanism in Li⁺ containing non-aqueous solvents takes place in two major steps. The first step is the formation of superoxide (O²⁻), which combines with Li⁺ and surface-adsorbed LiO_{2(ads)} and/or soluble LiO_{2(sol)} in the solution are formed. The produced discharge intermediates experience another electron transfer on the surface of the electrode or a disproportionation reaction in the solution to form solid product, Li₂O₂, as shown in Reactions (2)–(4) [103].



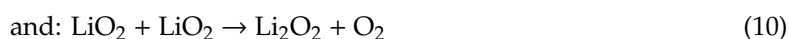
The reaction mechanism and intermediates (Li₂O₂) produced upon charging OER remain unclear. Peng et al. in their study excluded LiO₂ as the reaction intermediate during charging in acetonitrile, based on the absence of LiO₂ in the in situ surface-enhanced Raman spectroscopy (SERS) upon the charging process, instead, a direct two-electron process was proposed (Reaction (5)) [103].



Another density functional theory proposed a superficial reaction way to produce off-stoichiometric based on topotactic delithiation of Li₂O₂ (Reactions (6) and (7)) [103].



The experimental study utilized operando XRD showing that Li₂O₂ is oxidized through delithiation and form Li-deficient solid-solution (Li₂xO₂) phase in the tetraethylene glycol dimethyl ether solvent (Reactions (8)–(10)) [103]. The main variance among Li₂O₂-oxidation mechanisms lies on the type of the major charging reaction intermediate species.



Among rechargeable batteries, Li-air batteries substituted the costly counterparts based on their compactness, low weight, and cost-effective because they espouse inexpensive and light oxygen during discharge. In Li-air batteries, air cathode prerequisite serious focus because of sluggish kinetics of ORR and OER, which is attributed to the low efficiency of catalysts. In order to get a drastically improved performance of lithium-air batteries an efficient catalyst needs to be integrated to attain lesser polarization. Therefore, to attain commercialized lithium-air batteries, the development of highly efficient catalysts for the ORR and the OER in air cathode should be a point of interest. The bifunctional catalysts could instantaneously enable the ORR and OER contributing to great progressions in the Li-air battery performance. The promising techniques to develop MOF-derived catalysts for Li-air batteries will be discussed in the upcoming section [104,105].

3.2.1. MOF-Derived Metals/Metal Oxides/Metal Carbides Based Catalysts

To develop effectively and established cathode catalysts to tackle the sluggish kinetics of the ORR/OER processes in Li-air batteries, MOF-derived metal oxides appeared as promising candidates. Considering that performance evaluation for Li-O₂ battery occurs by electrochemical reactions occurring on the cathode, nanostructured advanced cathode materials designed for high energy densities have been developed. A novel and self-standing catalyst framework, where cobalt-based metal-organic framework (Co-MOF) was developed by 3D-printing to developed porous network geometry, was subjected to thermal annealing afterward. The exclusive framework provides effective deposition of Li₂O₂ particles during charging and then accelerates the decomposition of these insulating Li₂O₂ particles; this is attributed to the detention within well-controlled pores and the existence of Co-based electrocatalysts. The carbon framework itself possesses excellent conductivity and the required mechanical stability makes it a suitable conducting matrix. Consequently, the development of the porous matrix to self-standing catalyst construction can considerably raise the specific energy along with high energy density value up to 798 Wh kg⁻¹cell. Constructing 3D printed MOF-derived framework cathodes provides an alternate new way to an enhanced practical, specific energy of the Li-O₂ batteries [106].

An oxygen electrode was fabricated by stocking metal particles on the surface of porous carbon for Li-O₂ batteries. But nanoparticles are prone to lose contact during the reversible liquid-gas-solid reactions. To overcome such a problem, (Ru-MOF)-derived carbon composite electrocatalyst was prepared with stereoscopic Ru nanoparticles that are dispersed inside the carbon matrix. The high cycling stability is ensured based on the regeneration of the surface by Ru nanoparticles exposure performing as new active sites after the interacting surface Ru is lost because of the detachment from the carbon oxidation during operation. Ru/carbon electrocatalyst construction prepared using Ru-MOF crystals as a precursor established stable charge-discharge cycling performance with 800 cycles for 107 days at normal room temperature and current density of 500 mA/g and potentials 0.2/0.7 V (Figure 8a). It establishes a new window for the development of a better oxygen electrode of lithium-oxygen batteries (LOBs) [107].

MOFs as hybrid materials combining metal ions and organic ligands and having high porosity and vigorous structures have lately been anticipated as striking templates and precursors for manufacturing energy materials [108,109]. MOF-derived metal-nitrogen-carbon (M-N-C) catalysts gained massive attention because of high catalytic activity and low-cost for ORR and OER. Studies revealed that cathode catalysts with hierarchical porous structures significantly improve the performance of Li-O₂ batteries [110,111]. The metal-nitrogen (M-N_x) type efficiently provided active sites and enhanced the electric conductivity of the catalyst. However, a deficiency of balanced nanostructure production of the carbon catalyst makes the loaded metal nanoparticles cumulate during pyrolysis when the temperature is raised.

Hou et al. practiced vacancy engineering techniques to fabricate 2D micro-assembly Co₃O₄ nanosheets. The contents of oxygen and metal ions vacancy were adjusted by changing annealing temperature. It was found that the synergistic effects of the contents enhanced the electrochemical

performance of the Li–O₂ battery. The study revealed that the highest number of defects led to premier electrochemical performance and displayed a discharge capacity of 8000 mAh/g along with electrochemical stability for more than 300 cycles under a specific capacity limit of 600 mAh/g at a current density of 100 mA/g. The concentration of oxygen vacancies in Co₃O₄ rises with increasing the annealing temperature from 200–400 °C, with the highest defects observed at 300 °C. The concentration of the structural defects controlled the electrocatalytic performances for Co₃O₄ since these defects provide rails for O₂ to pass into 2D micro-assembly Co₃O₄ nanosheets (Figure 8b) and it creates active sites that speed up ORR through the discharge procedure which facilitates to greater cycling stability. Electrocatalytic performances are also improved by ambient oxygen vacancies present in Co₃O₄ which assist mass transportation in speeding up the reaction between Li⁺ and O₂ when ORR is happening and facilitates the deposition of Li₂O₂ films. This study opened new prospects to design transition-metal oxides as cathode materials for potential Li–O₂ batteries [112].

In recent research work, the unique thermal and electrical conduction characteristics along with outstanding surface physicochemical features of the transition metal carbides (TMCs) made them the focus of attention [113,114]. Several carbides were utilized to enhance catalytic performance and activity, among them, molybdenum carbides were studied mostly by virtue of their high electrical conduction properties and distinctive d-band electronic structures. Mo₂C and MoC got special interest as bifunctional catalysts in Li–O₂ for both ORR and OER reactions. The activity and permanence of Pt-based ORR electrocatalysts took a prominent enhancement by using MoC catalysts [115]. CNT as effective conductive materials for MoC_x, specifically heteroatom-doped CNTs doped with metals and nitrogen exhibited enhanced catalytic activity. N-doped CNT-encapsulated Co nanoparticles catalyst exhibited exceptional stability and excellent electrochemical activity in ORR. A bifunctional catalyst containing molybdenum carbide nanorods grafted with N-doped CNTs (NCNTs) was developed to stretch the electrochemical properties of Li–O₂ batteries. MoO₃ nanorods were coated with a Co-based ZIF-67 and treated to get MoC–Mo₂C/NCNTs nanocatalyst. The as-obtained nanorods have a distinctive structure that offers a large number of active sites and ample space for managing Li₂O₂ along with facilitating electrons transport via the catalytic active NCNT conductive paths. The synergetic effects of the three components Co, MoC, and NCNT considerably enhanced electrocatalytic performance of the composite catalyst in ORR and OER in Li–O₂ batteries. An extraordinary specific discharge capacity of 34,862 mAh/g at current density 200 mA/g and cyclic stability of 162 cycles having a current density of 200 mA/g also considerably deprived discharge–charge overpotential. These results propose that the composite nanorod is an effective, steady bifunctional catalyst for potential Li–O₂ batteries [116].

3.2.2. MOF-Derived Bimetallic and Hybrid Catalysts

MOFs, its derivatives, and composites are enormously used as air electrodes and exhibited a greater discharge capacity attributed to its high specific surface area, distinct porous structure, and adequate active sites [117,118]. Recently, transition metal oxides/metal oxides appeared as a prominent constituent of Li–O₂ batteries air cathode. Co₃O₄- and NiCo₂O₄-based catalysts exhibited good ORR/OER activity and improved cathodic performance. The Li–O₂ batteries based on single transition metal oxides suffer from poor specific capacity, insufficient cycling life, and small catalytic activity. Hence, a hybrid electrode with a synergistic effect between its components can increase the catalytic performance of the cathode. For instance, a bifunctional catalyst-based nanoplatelet was synthesized with MnO₂-modified Co₃O₄ for Li–O₂ battery, where it displayed better electrochemical properties in comparison to the single component electrode [104].

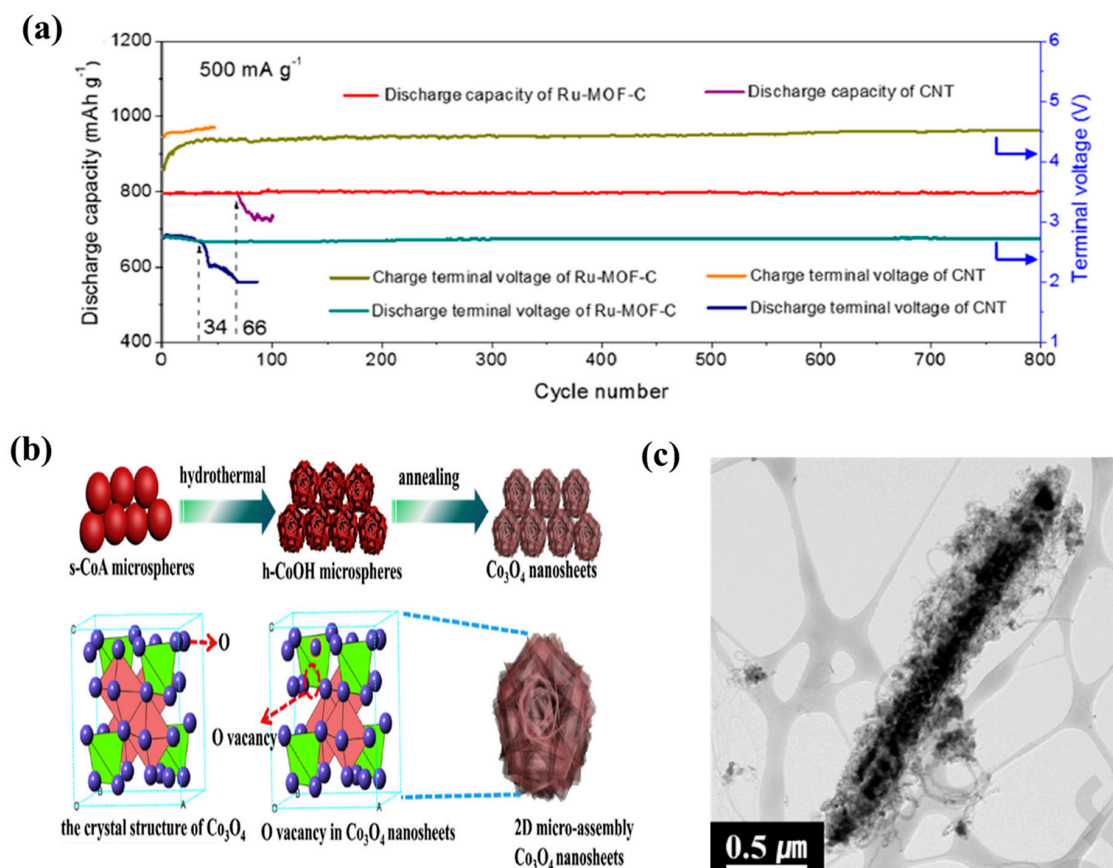


Figure 8. (a) The discharge capacities of the LOBs with Ru-MOF-C and CNT as the catalyst at a current density of 500 mA/g [107]. (b) The schematic representation of the synthetic procedure for 2D micro-assembly Co₃O₄ nanosheets [112]. (c) MoC-Mo₂C/NCNTs nanorods TEM image at 0.5 μm amplitude [116].

A hierarchical porous structure having microporous channels will enable fast O₂ diffusion. The mesopore structure can efficiently increase the electrolyte immersion whereas the macroporous one enables the kinetic availability of the active sites and accumulates additional discharge products. Nevertheless, most air-electrodes mentioned with macropores are metal oxides, and a very small proportion of bimetal-nitrogen-carbon (BM-N-C) materials derived from micro-meso-macroporous MOFs applied as the cathode of Li-O₂ batteries. However, a bifunctional catalyst, micro-meso-macroporous FeCo-N-C-X derived from hierarchical M-FeCo-ZIFs-X was synthesized (Figure 9a). Polystyrene microspheres templates were used, hierarchical M-FeCo-ZIFs-X worked as precursors, and after etching the templates M-FeCo-ZIFs-X nanoparticles with evenly distributed macropores were attained. M-FeCo-N-C-0.2-based cathode showed a high initial capacity of 18,750 mAh/g at a current density of 0.1 A/g and exhibited good rate capability of 7900 mAh/g at a current density of 0.5 A/g after 192 cycles of stable performance. The exceptional performance accredited to the synergistic effect of Fe, Co nanoparticles, and N co-doping carbon frameworks having distinct micro-meso-macroporous structure [119].

Another free-standing array structured Co₃O₄@NiCo₂O₄ cathode prepared by in situ growth of cobalt-based metal-organic framework (Co-MOF) sheets on carbon cloth (CC) and impregnation in nickel nitrate solution followed by pyrolysis under air-flow. The free-standing and binder-free Co₃O₄@NiCo₂O₄/CC cathode displayed extraordinary ORR/OER activity and greater cycling stability, a specific capacity of 10,645 mAh/g (Figure 9b), and stability of 225 cycles without obvious degradation were achieved [120]. With the same vision, in Li-O₂ batteries, metal/metal oxide composite catalyst (Fe₂O₃@C/MnO₂) which combine Fe₂O₃ and MnO₂ displayed enhanced cycling performance and reduced charge voltage than single C and Fe₂O₃@C electrodes [121].

Zhang et al. designed and synthesized the metal hybrid catalyst Mn-MOF-74@CNTs as a cathode material for Li–O₂ batteries where Mn-MOF-74 nanoparticles were grown directly on carbon nanotubes using additive-mediated synthesis method. The formation of less-reactive discharge product LiOH compared to Li₂O₂ by the nano-architected Mn-MOF-74@CNTs hybrid catalyst, Mn-MOF-74@CNTs-based oxygen cathode display fewer side reactions. The formed cathode displayed improved cycling performance even in a humid oxygen atmosphere where Li₂O₂ was made as discharge products [122].

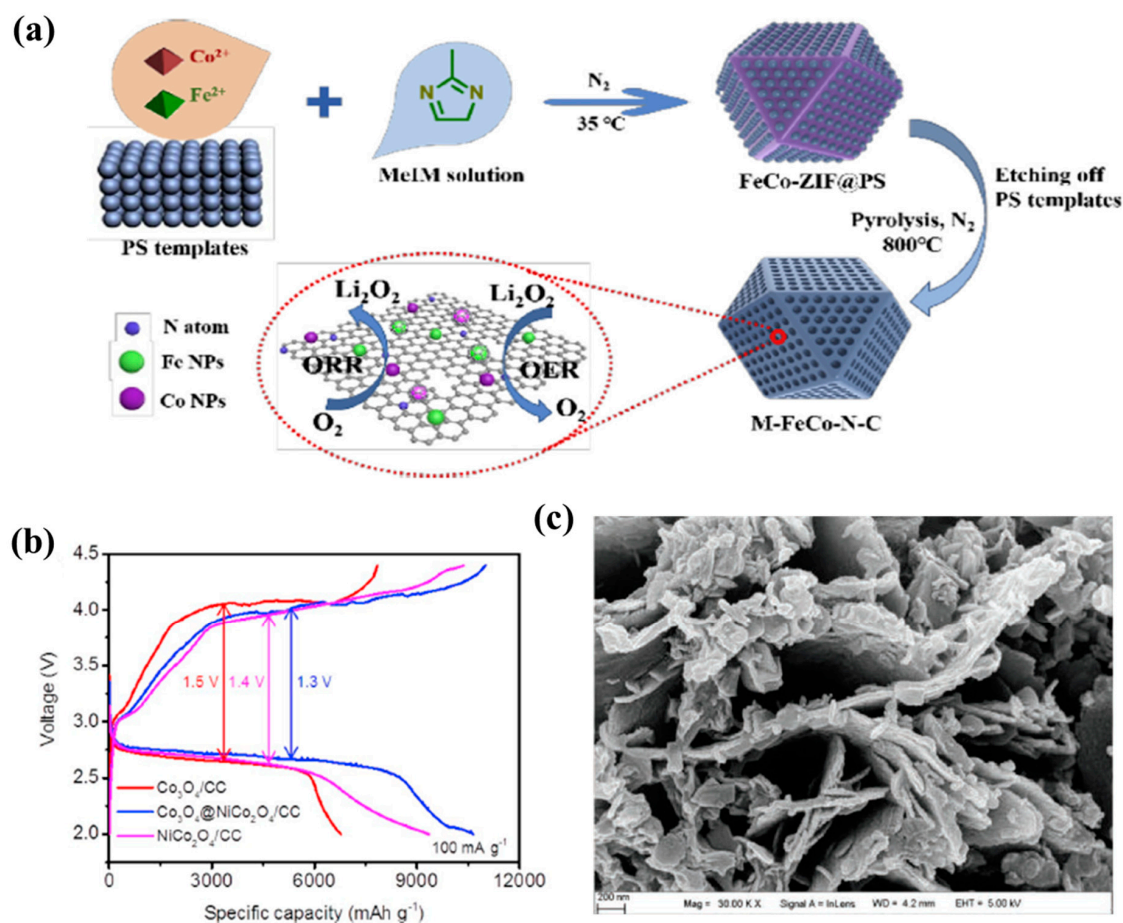


Figure 9. (a) The illustration of the synthetic process of M-FeCo-N-C-X catalysts [119]. (b) The first discharge–charge curves of Co₃O₄/CC, Co₃O₄@NiCo₂O₄/CC, and NiCo₂O₄/CC catalysts [120]. (c) The FESEM image of 1MIL/40ZIF-1000 [123].

Dual metal–organic frameworks mixture containing MIL-100(Fe) and ZIF-8, was thermally activated in N₂ and then in NH₃ (Figure 9c). The subsequent catalysts demonstrated stacked carbon nanosheets (CNSs) morphology with a minor portion of carbon nanotubes (CNTs) protruding from the surface. The carbon matrixes were doped evenly with Fe and N species, and the present additional Fe generates Fe–Fe₃C particles to improve oxygen affinity and indorse *OH desorption. The formed catalyst exhibits outstanding ORR catalytic performance in alkaline/acidic half-cells, along with a PEMFC and also an aprotic Li–O₂ battery. The exceptional ORR catalytic presentation attributed to Fe–Fe₃C@Fe–N–C dual active sites, hierarchical porosities (micro/macropores) for bulk transport, and partial carbon graphitization for rapid charge transfer. These outcomes establish MOFs as model systems for the rational design of electrocatalyst for energy-based functional applications [123].

One-step carbonization was used to synthesize core@shell-structured, hierarchically porous manganese oxide/cobalt manganite@nitrogen-doped carbon (MnO/CoMn₂O₄@N–C) nanorods with interstitially decorated CoMn₂O₄ nanoparticles. MOF-coated with α -manganese oxide (α -MnO₂@ZIF-67) nanorods

cathodes were used for LOBs to enhance the bifunctionality, cyclability of α - MnO_2 nanorod cathode-based LOBs along with specific discharge capacity. $\text{MnO}/\text{CoMn}_2\text{O}_4@\text{N-C}$ nanorod cathode-based LOB shows a higher full specific discharge capacity of 8625 mAh/g and cyclability of 48 discharge–charge cycles at 200 mA/g specific current and 2000 mAh/g limited specific discharge capacity compared to their α - MnO_2 nanorod equivalents. Alike MOF-derived nanoparticle-decorated nano-constructions lead to high-performance tunable bifunctional electrocatalysts [124].

Inquest to produce efficient and stable catalysts, composites made of carbon with embedded metal/metal oxides fascinated great attention as electrochemical catalysts. However, intensive carbon evaporation during the pyrolysis synthesis causes reduced dispersion of the active sites and lower catalytic stability, to tackle the particles aggregation engendered an oxide shell was coated on precursor under high temperature. Liang et al. used Zn, Co zeolite imidazole skeleton coated by mesoporous silica functioned as precursor followed by pyrolyzation and Co, NeCNF catalyst was synthesized. Bimetallic Co, NeCNF catalyst has heteroatoms that demonstrate synergistic effects with other functional components that significantly enhance catalytic activity. The outstanding electrochemical performance with a high specific capacity of 5288 mAh/g along with outstanding cycle stability without substantial voltage reduction after 500 cycles was attained. The exclusive core-shell structure and metallic cobalt active sites contribute to excellent electrochemical properties [125].

3.2.3. Non-Metallic MOF-Derived Carbon Dopants

Noble metal and metal oxides, and hybrid showed excellent catalytic activities, but their practical applications got limitation owing to their high cost. Developing proficient electrocatalysts with efficient structure is expected to be achieved to reduce the problems related to Li_2O_2 discharge products during the ORR/OER in Li-O_2 batteries. It will not only overcome the deprived rate capability but also increase the electrochemical properties of the LOB. Yu et al. reported the synthesis of cobalt nanoparticle in situ encapsulated into nitrogen-doped carbon polyhedral under an Ar atmosphere, where ZIF-67 pyrolysis was conducted at a temperature between 700–1000 °C and optimal temperature of 900 °C was found. The as-prepared Co@NC and Co@NC-900/acetylene black material was implemented as bifunctional electrocatalysts and used as an oxygen electrode in Li-O_2 batteries. The cathode displayed discharge abilities of 3110 mAh/g and stable cycle life for more than 80 cycles along with the limiting capacities of 1000 mAh/g. The Co@NC-900/AB electrode could be attributed as potential metal-based cathode electrocatalysts because of its electrical conductivity, suitable N content, large surface area, and numerous active sites in Li-O_2 batteries [126].

Thi et al. have reported a dual-phase carbon nanostructure for lithium–oxygen battery cathodes, by interlaced linkage of MOF-derived carbon and conductive carbon nanotubes. Carbonized MOF transforms into high porous carbon, the formation of an effective and high capacity cathode. Dual-phasic carbon nanostructure was constructed by growing MOF nanoparticles on the CNTs followed by the carbonization of MOF/CNTs. The formed structure includes the benefits of both components, MOF-C offers a large surface area, while CNTs deliver superficial pathways. Dual-phasic carbon cathode exhibited that the synergistic nanoarchitecture of material demonstrated a high discharge capacity of 10,050 mAh/g along with stable cycling performance over 75 cycles showing excellent electrochemical performance of LOBs [119].

3.3. Al-Air Batteries

Other active metals have been utilized as anodes for air batteries including Ca, Mg, Al, and Fe [127–129]. Aluminum (Al), a popular existing anode material for metal fuel cells and air batteries application, has a great advantage over other metals like its abundance, reasonable price, non-toxic nature, environment friendliness, and recyclability making Al a promising candidate for next-generation energy storage equipment [130,131]. Al appeared as ideal material based on properties; it acquired like its trivalence and low atomic weight of 26.98g/mol, Al only lags behind Li in its theoretical specific capacity value that is 2.89 A.h/g. Moreover, by a value of 8.04 A.h.cm³, the theoretical specific

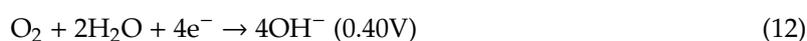
volumetric capacity of Al is the highest among the metallic fuels making it special [131,132], the first Al-air battery was developed in the 1960's by Zaromb and it emerged as an efficient source with several applications [133]. Using Al-air as electric vehicle power by Alcoa and Phinergy company made it prominent in 2014. Nevertheless, the commercialization of Al-air batteries is still in development stages because of the high corrosion rate of Al anode in alkaline electrolytes and the polarization factor in neutral electrolytes because of insoluble oxide film formed on Al anode [134,135].

A characteristic Al-air battery is generally composed of three components, an Al anode, an air cathode, and an alkaline or brine electrolyte. The half-cell reactions on both electrodes are shown in (Reaction (11,12)), whereas overall Al-air battery reactions can be summarized as shown in (Reaction (13)). The parasitic hydrogen evolution effect at the Al anode is shown in (Reaction (14)) [136,137].

Anode:



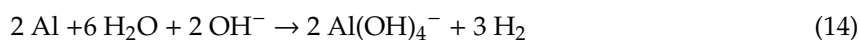
Cathode:



Overall reaction:



Parasitic reaction:



MOF-Based Electrocatalysts for Al-Air Battery

The sluggish kinetics of cathodic ORR limits the power density of Al-air batteries. Electrocatalysts are vital for oxygen reduction reaction owing to involvements of multiple adsorption/desorption reactions where ORR undertakes in the "four-electron" pathway and produces extraordinary current efficiency and discharge voltage. To effectively increase active sites and speed up mass transfer, one could deploy metal content in a porous carbon matrix. The matrix restricts aggregation of metals to enhance ORR performance by more exposure of active sites to the interface. MOFs are considered as the favorite precursors to prepare carbon matrix [138–140]. Silica stabilizing technique was used to develop a stable and efficient electrocatalyst where CoNi bimetal nanoalloy is uniformly embedded in N-doped carbon framework for Al-air batteries. The etching process followed by silica stabilization generates pores in the produced CoNi-NCF (nitrogen-doped carbon framework) electrocatalyst. A large number of active sites in CoNi nanoalloy, porous structure, high specific surface area, and stable conductive carbon matrix made the CoNi-NCF exhibit excellent ORR performance. A half-wave potential of 0.91 V was achieved in 0.1 M KOH solution and 0.64 V in 3.5 wt% NaCl solution. When CoNi-NCF was employed as a cathode catalyst in aqueous and solid flexible Al-air batteries, active sites improved the ORR performance and highest discharge performance, and longtime durability and high flexibility were achieved [141].

Liu et al. developed bimetallic spinel-type hollow nanocages (ZnO/ZnCo₂O₄/C) derived from the ZIF-67/GO/Zn(NO₃)₂ precursors. The ZIF-67 helped in obtaining a hollow cage structure with more active sites and a higher surface area. The active sites and surface area were further enhanced by the dispersion of MOF particles on reduced GO. The presence of rGO in the hybrid structure enhances the overall electrical conductivity and leads to a better performance in the battery [142]. Cu-centered MOF precursor was used to modifying the Ketjenblack (KB) carbon to make a novel hybrid catalyst. The synergistic effect between crystalline Cu/Cu₂O nanoparticles and noncrystalline CuN_xC_y species, produced by the calcination, enhanced the catalytic activity of the modified KB carbon toward ORR. The excellent performance of the as-manufactured hybrid catalyst was exhibited, where half-wave potential and larger limiting-current density was shown compared to 20%wt Pt/C. A high stable

voltage of 1.53 V at a working current density of 40 mA/cm² was marked on the home-made Al–air batteries [143].

A simple double-phase encapsulation and post heat treatment method was used to structure a hierarchical porous N, S-co-doped carbon where cobalt-nickel-sulfide nanoparticles are encapsulated inside. Integrated hybrid architecture Ni-Co-S@G/NSC displayed an onset potential of 0.94 V, a greater discharge voltage plateau, enhanced stability, and half-wave potential to the commercial Pt/C catalyst in ORR and the full battery test. Superior ORR activity of the Ni-Co-S@G/NSC catalyst credited to greater surface area and pore volume and synergetic effect of the components. MOFs with a double-phase encapsulation approach contribute to design improved catalysts for Al-air batteries [144].

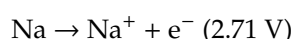
3.4. Na-Air Battery

Among hereby reported metal-air batteries, Na exhibit relatively high theoretical values for specific energy where lithium-air batteries are catching up with the theoretical specific energy of gasoline. Factors like ingestion of solvent in the discharging process, blockage of pores, and the air cathode degradation and degradation of the air cathode limit the commercial success of Li-air batteries [145,146]. Na metal-based batteries appeared as a prospective substitute to lithium-based batteries because of its alike electrochemical features [147,148]. Sodium appeared as the most emerging replacement for lithium to meet the requirement of energy storage owing to its abundance in earth crust as the forth plentiful element sharing approximately 2.6% sodium by weight, as well as the easy availability and low cost [149,150].

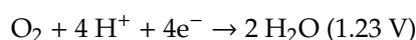
The reduction potential of 230 mV of sodium makes it store more energy owing to the fact that cells can produce large potential. Moreover, low atomic weight and higher electronegativity enable delivering high specific capacity. Combining metallic sodium with oxygen as an opponent reactant at the cathode provides the basis for Na-air batteries. The Na–air battery is counted as an environment-friendly electrochemical power storage device with developed energy density [151]. The value 1600 Wh kg^{−1} of specific capacity in Na-air batteries is not as high as that of Li-air batteries but it is suitable for several devices in this range of capacity. The Na–air battery is made of Na metal anode and an air cathode where oxygen is taken from the environment while discharging. Based on the electrolytes, Na-air batteries are divided into two types; nonaqueous and aqueous [152].

The charge-discharge mechanism for the electrolytic based hybrid Na-air battery can be explained by the following reactions: [153].

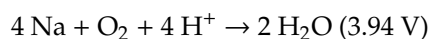
Anode:



Cathode:



Overall reaction:



The discharge products for Na–air batteries are diverse, where sodium superoxide (NaO₂) is the chief discharge product. The development of Na₂O₂, another discharge product, is thermodynamically preferred than NaO₂, but looking at the perspective from a kinetic point of view NaO₂ only needs a one-electron transfer that is comparatively easy to have. NaO₂ is reflected as an electronic conductor showing various properties for the charging process [154].

The ORR and OER process in Na-air batteries face hinders from slow kinetics while undergoing discharge and charge process and produces a high overpotential gap [155,156]. A stable and active bifunctional electrocatalyst is highly demanded to promote the efficiency of hybrid Na–air battery and noble metal catalysts like Pt and Pt–based materials regarded as effective catalysts. However, higher cost, poor stability, and other factors made high demand to produce effective bifunctional electrocatalysts [157,158]. MOF and MOF-derived materials were extensively used owing to their

superior surface area, hierarchical pores, and available functionalization for electrochemical catalysis of ORR and OER.

MOF-Based Electrocatalysts for Na-Air Battery

MOF-derived Co nanoparticles confined in N-doped carbon nanotubes were utilized in Na-air battery, which exhibited excellent electrochemical performance. The well-developed porous structure and the higher number of active sites along with the synergetic effect of the components, i.e., N dopants and Co nanoparticles, made it perform efficiently in ORR and OER in Na-air batteries [158]. ZnCo bimetal organic framework (bi-MOF) was used to design exceptional extremely discrete Co nanoparticle decorated on N-doped defective carbon nano-framework (Co-N-C). Zinc evaporation results in a higher specific surface area that accelerates the adsorption and desorption of oxygen, leading to easy access catalytic sites. The ORR and OER can be processed with ease because of N-doped defective carbon and coexistence of CoN_x and Co set which perform as active sites. Interface electron transfer was facilitated by the Co nanoparticles and carbon materials where rich Co-N-C species perform as durable bridging bonds. The large number of active sites, improved electrons transmission, and the synergetic coupled effect resulted in a low overpotential gap of 0.94 V between the OER potential and ORR. The half-wave potential exhibited excellent electrocatalytic performance. The Co-N-C-0.5 catalyst resulted in a low voltage gap of 0.31 V in Na-air battery where the round trip efficiency of 90.0% was attained at the current density of 0.1 mA/cm² along with an excellent cycle rate for charge and discharge [159].

The hierarchical $\text{Co}_3\text{O}_4@\text{MnCo}_2\text{O}_{4.5}$ nanocubes having a hollow cage type assembly was prepared and utilized in Na-O₂ batteries as an effective air cathode catalyst. Three steps were used for synthesis, including templating with MOFs to assist synthetic route, surface etching, and high-temperature annealing. The yolk like structural design, superior surface area, a large number of active sites, and improved conductivity for electron diffusion in h- $\text{Co}_3\text{O}_4@\text{MnCo}_2\text{O}_{4.5}$ along with macropores and mesopores uniformly dispersed on the surface, provide effective O₂ diffusions pathways and enormously increase catalytic activity during the ORR and OER. The discharge product deposits on the surface of h- $\text{Co}_3\text{O}_4@\text{MnCo}_2\text{O}_{4.5}$ result in relatively loose morphology, which is favorable for the efficient reversibility of the Na-O₂ battery. Higher cyclic stability and efficiency enhancements in discharge-charge overpotential were achieved in Na-air batteries based on h- $\text{Co}_3\text{O}_4@\text{MnCo}_2\text{O}_{4.5}$ [160].

4. Conclusions

As energy continues to be one of the pivotal issues of the century, metal-air batteries are hereby discussed because of their solid position as a candidate for renewable energy storage, specifically solar energy, being the most attractive renewable energy source. The latest publications involving prominent synthesis methods and engineering strategies to fabricate outstandingly efficient MOFs were selected and elaborated in this review. This review endeavored to shed light on their vast potential as efficient functional materials for solar cells and metal-air batteries, combining most essential features; larger surface and area and highest conductivity. MOF-derived carbon materials are also reported to provide a wide dispersion of versatile active sites ranging from metal, metal oxides, or non-metals, to further promote catalysis of oxygen reactions. This promising class of materials would successfully reduce the gap between energy-related discoveries made inside laboratories and the industrial sector.

Author Contributions: M.E.H., A.R.A., H.A.Y.: Article writing; A.A., N.H., and F.V.: Directing. Discussion; F.V.: final review and editing. All authors have read and agreed to the published version of the manuscript.

Funding: This research received no external funding.

Acknowledgments: The authors would like to acknowledge State Key Laboratory of Advanced Technology for Materials Synthesis and Processing, Wuhan University of Technology. M.E.H. expresses his deep appreciation to the Chinese Scholarship Council (CSC) for his Ph.D. study grant no. 2017GXZ001124.

Conflicts of Interest: The authors declare no conflict of interest.

References

1. Shaker, M.T.; Khedr, A.E.; Kholeif, S. A Proposed Framework for Reducing Electricity Consumption in Smart Homes using Big Data Analytics. *J. Comput. Sci.* **2019**, *15*, 537. [[CrossRef](#)]
2. Kumari, A.; Tanwar, S.; Tyagi, S.; Kumar, N.; Obaidat, M.S.; Rodrigues, J.J.P.C. Fog Computing for Smart Grid Systems in the 5G Environment: Challenges and Solutions. *IEEE Wirel. Commun.* **2019**, *26*, 47. [[CrossRef](#)]
3. Apostolaki-Iosifidou, E.; Woo, S.; Lipman, T. Challenges and Opportunities for Electric Vehicle Charging Detection Using Utility Energy Consumption Data. In Proceedings of the Transportation Research Board Annual Meeting, Washington, DC, USA, 13–17 January 2019. No. 19-05695.
4. IEA. Electricity. In *World Energy Outlook*; IEA: Paris, France, 2019.
5. Gurung, A.; Qiao, Q. Solar Charging Batteries: Advances, Challenges, and Opportunities. *Joule* **2018**, *2*, 1. [[CrossRef](#)]
6. Tenfen, D.; Finardi, E.C.; Delinchant, B.; Wurtz, F. Lithium-ion Battery Modelling for the Energy Management Problem of Microgrids. *Inst. Eng. Technol.* **2016**, *10*, 576. [[CrossRef](#)]
7. Li, Y.; Lu, J. Metal-Air Batteries: Will They Be the Future Electrochemical Energy Storage Device of Choice? *ACS Energy Lett.* **2017**, *2*, 1370. [[CrossRef](#)]
8. Li, Q.; Liu, Y.; Guo, S.; Zhou, H. Solar Energy Storage in the Rechargeable Batteries. *Nano Today* **2017**, *16*, 46. [[CrossRef](#)]
9. Davari, E.; Ivey, D.G. Bifunctional Electrocatalysts for Zn–Air Batteries. *Sustain. Energy Fuels* **2017**, *2*, 39. [[CrossRef](#)]
10. Fiakas, C.D. Metal-Air Battery Stocks. *ALT Energy Stocks*, 4 April 2013.
11. Corma, A.; Garcá, H.; Xamena, F.X.L.I. Engineering Metal Organic Frameworks for Heterogeneous Catalysis. *Chem. Rev.* **2010**, *110*, 4606. [[CrossRef](#)]
12. Hönicke, A.I.; Senkovska, I.; Bon, V.; Baburin, I.; Boenisch, N.; Raschke, S.; Evans, J.D. Balancing Mechanical Stability and Ultrahigh Porosity in Crystalline Framework Materials. *Angew. Chem. Int. Ed.* **2018**, *57*, 13780. [[CrossRef](#)]
13. Lee, J.; Farha, O.K.; Roberts, J.; Scheidt, K.A.; Nguyen, S.T.; Hupp, J.T. Metal–Organic Framework Materials as Catalysts. *Chem. Soc. Rev.* **2009**, *38*, 1450. [[CrossRef](#)]
14. Schram, W.L.; Lampropoulos, I.; van Sark, W.G.J.H.M. Photovoltaic Systems Coupled with Batteries that are Optimally Sized for Household Self-Consumption: Assessment of peak shaving potential. *Appl. Energy* **2018**, *223*, 69. [[CrossRef](#)]
15. Spoerke, E.D.; Small, L.J.; Foster, M.E.; Wheeler, J.; Ullman, A.M.; Stavila, V.; Rodriguez, M.; Allendorf, M.D. MOF-Sensitized Solar Cells Enabled by a Pillared Porphyrin Framework. *J. Phys. Chem. C* **2017**, *121*, 4816. [[CrossRef](#)]
16. Chen, T.; Huang, Y.; Li, C.; Kung, C.; Vittal, R.; Ho, K. Metal-Organic Framework/Sulfonated Polythiophene on Carbon Cloth as a Flexible Counter Electrode for Dye-Sensitized Solar Cells. *Nano Energy* **2016**, *32*, 19. [[CrossRef](#)]
17. Ahmed, A.S.A.; Xiang, W.; Amiin, I.S.; Zhao, X. Zeolitic-Imidazolate-Framework (ZIF-8)/PEDOT: PSS Composite Counter Electrode for Low Cost and Efficient Dye-Sensitized Solar Cells. *New J. Chem.* **2018**, *42*, 17303. [[CrossRef](#)]
18. Shen, D.; Pang, A.; Li, Y.; Dou, J.; Wei, M. Metal–Organic Frameworks at Interfaces of Hybrid Perovskite Solar Cells for Enhanced Photovoltaic. *Chem. Commun.* **2018**, *54*, 1253. [[CrossRef](#)]
19. Xing, W.; Ye, P.; Lu, J.; Wu, X.; Chen, Y.; Zhu, T.; Peng, A. Tellurophene-Based Metal-Organic Framework Nanosheets for High- Performance Organic Solar Cells. *J. Power Sources* **2018**, *401*, 13. [[CrossRef](#)]
20. O'Regan, B.; Gratzel, M. High-Efficiency Solar Cell Based on Dye-Sensitized Colloidal TiO₂ Films. *Lett. Nat.* **1991**, *353*, 737. [[CrossRef](#)]
21. Hagfeldt, A.; Boschloo, G.; Sun, L.; Kloo, L.; Pettersson, H. Dye-Sensitized Solar Cell. *Chem. Rev.* **2010**, *110*, 6595. [[CrossRef](#)]
22. Sharma, K.; Sharma, V.; Sharma, S.S. Dye-Sensitized Solar Cells: Fundamentals and Current Status. *Nanoscale Res. Lett.* **2018**, *13*, 381. [[CrossRef](#)]
23. Yeoh, M.; Chan, K.-Y. Recent Advances in Photo-Anode for Dye-Sensitized Solar Cells: A review. *Energy Res.* **2017**, *13*, 381.

24. Aghazada, S.; Nazeeruddin, M.K. Ruthenium Complexes as Sensitizers in Dye-Sensitized Solar Cells. *Inorganics* **2018**, *6*, 52. [[CrossRef](#)]
25. Ammar, A.M.; Mohamed, H.S.H.; Yousef, M.M.K.; Abdel-hafez, G.M.; Hassanien, A.S.; Khalil, A.S.G. Dye-sensitized solar cells (DSSCs) based on extracted natural dyes. *Hindawi* **2019**, *2019*, 1867271. [[CrossRef](#)]
26. Iftikhar, H.; Sonai, G.G.; Hashmi, S.G.; Fl, A.; Lund, P.D. Progress on Electrolytes Development in Dye-Sensitized Solar Cells. *Materials* **2019**, *12*, 1998. [[CrossRef](#)] [[PubMed](#)]
27. He, Y.; Zhang, Z.; Wang, W.; Fu, L. Metal Organic Frameworks Derived High-Performance Photoanodes for DSSCs. *J. Alloys Compd.* **2020**, *20*, 154089. [[CrossRef](#)]
28. Li, Y.; Pang, A.; Wang, C.; Wei, M. Metal–Organic Frameworks: Promising Materials for Improving the Open Circuit Voltage of Dye-Sensitized Solar Cells. *J. Mater. Chem.* **2011**, *21*, 17259. [[CrossRef](#)]
29. Gu, A.; Xiang, W.; Wang, T.; Gu, S.; Zhao, X. Enhance Photovoltaic Performance of Tris(2,20-bipyridine) Cobalt (II)/(III) based Dye-sensitized Solar Cells via Modifying TiO₂ Surface with Metal-Organic Frameworks. *Sol. Energy* **2017**, *147*, 126. [[CrossRef](#)]
30. Alwin, S.; Ramasubbu, V.; Shajan, X.S. TiO₂ Aerogel–Metal Organic Framework Nanocomposite: A New Class of Photoanode Material for Dye-Sensitized Solar Cell Applications. *Bull. Mater. Sci.* **2018**, *41*, 27. [[CrossRef](#)]
31. Maza, W.A.; Haring, A.J.; Ahrenholtz, S.R.; Epleya, C.C.; Lina, S.Y.; Morris, A.J. Ruthenium(II)-Polypyridyl zirconium(IV) Metal-organic Frameworks as A New Class of Sensitized Solar Cells. *Chem. Sci.* **2015**, *7*, 719. [[CrossRef](#)]
32. Wu, J.; Lan, Z.; Lin, J.; Huang, M.; Huang, Y.; Fan, L.; Luo, G.; Lin, Y.; Xie, Y.; Wei, Y. Counter Electrodes in Dye-Sensitized Solar Cells. *Chem. Soc. Rev.* **2017**, *46*, 5975. [[CrossRef](#)]
33. Jin, Z.; Zhang, M.; Wang, M.; Feng, C.; Wang, Z. Metal Selenides as Efficient Counter Electrodes for Dye-Sensitized Solar Cells. *Acc. Chem. Res.* **2017**, *50*, 895. [[CrossRef](#)]
34. Gnanasekar, S.; Kollu, P.; Jeong, S.K.; Grace, A.N. Low-cost and Efficient Counter Electrode with Carbon Wrapped Vo₂(M) Nanofiber for Dye- Sensitized Solar Cells. *Sci. Rep.* **2019**, *9*, 5177. [[CrossRef](#)] [[PubMed](#)]
35. Kumar, R.; Sahajwalla, V.; Bhargava, P. Fabrication of A Counter Electrode for Dye-Sensitized Solar Cells (DSSCs) Using A Carbon Material Produced with the Organic Ligand 2-Methyl-8-Hydroxyquinolinol (Mq). *Nanoscale Adv.* **2019**, *1*, 3192. [[CrossRef](#)]
36. Li, G.; Gao, X. Low-Cost Counter-Electrode Materials for Dye-Sensitized and Perovskite Solar Cells. *Adv. Mater.* **2019**, *32*, 1806478. [[CrossRef](#)] [[PubMed](#)]
37. Zhang, J.; Zhou, H.; Zhou, D.; Liao, P. Controlling Flexibility of Metal–Organic Frameworks. *Natl. Sci. Rev.* **2018**, *5*, 907. [[CrossRef](#)]
38. He, A.H.; Sun, Q.; Gao, W.; Perman, J.A.; Sun, F.; Zhu, G.; Aguila, B.; Space, B.; Ma, S. A Stable Metal-Organic Framework Featuring Local Buffer Environment for Carbon Dioxide Fixation. *Angew. Chem. Int. Ed.* **2018**, *57*, 4657. [[CrossRef](#)]
39. Ma, X.; Chai, Y.; Li, P.; Wang, B. Metal–Organic Framework Films and Their Potential Applications in Environmental Pollution Control. *Acc. Chem. Res.* **2019**, *52*, 1461. [[CrossRef](#)]
40. Chueh, C.; Chen, C.; Su, Y.; Konnerth, H.; Gu, Y.; Kung, C.; Wu, K.C. Harnessing MOF Materials in Photovoltaic Devices: Recent Advances, Challenges, and Perspectives. *J. Mater. Chem. A* **2019**, *7*, 17079. [[CrossRef](#)]
41. Liu, S.; Li, Z.; Zhao, K.; Hao, M.; Zhang, Z.; Li, L.; Zhang, Y.; Zhang, W. A Facile Hydrothermal Synthesis of MoS₂@Co₃S₄ Composites Based on Metal Organic Framework Compounds as a High-Efficiency Liquid-State Solar Cell Counter Electrode. *J. Alloys Compd.* **2020**, *20*, 154910. [[CrossRef](#)]
42. Ou, J.; Xiang, J.; Liu, J.; Sun, L. Surface-Supported Metal-Organic Framework Thin-Film-Derived Transparent CoS_{1.097}@N-Doped Carbon Film as an Efficient Counter Electrode for Bifacial Dye-Sensitized Solar Cells. *ACS Appl. Mater. Interfaces* **2019**, *11*, 14862. [[CrossRef](#)]
43. Tian, Y.; Wang, Y.; Chen, S.; Gu, Z.; Zhang, J. Epitaxial Growth of Highly Transparent Metal-Porphyrin Framework Thin Films for Efficient Bifacial Dye-Sensitized Solar Cells. *ACS Appl. Mater. Interfaces* **2019**, *12*, 1078. [[CrossRef](#)]
44. Bella, F.; Bongiovanni, R.; Kumar, R.S.; Kulandainathan, M.A.; Stephan, A.M. Light Cured Networks Containing Metal Organic Frameworks as Efficient and Durable Polymer Electrolytes for Dye-Sensitized solar cells. *J. Mater. Chem. A* **2013**, *1*, 9033. [[CrossRef](#)]

45. Sarwar, S.; Lee, M.; Park, S.; Dao, T.T.; Ullah, A.; Hong, S.; Han, C. Transformation of A Liquid Electrolyte to A Gel Inside Dye Sensitized Solar Cells for Better Stability and Performance. *Thin Solid Film.* **2020**, *20*, 30236. [CrossRef]
46. Kojima, A.; Teshima, K.; Shirai, Y.; Miyasaka, T. Organometal Halide Perovskites as Visible-Light Sensitizers for Photovoltaic Cells. *JACS* **2009**, *131*, 6050. [CrossRef] [PubMed]
47. NREL Transforming Energy. Best Research-Cell Efficiencies Chart. *NREL* **2019**. Available online: <https://www.nrel.gov/pv/cell-efficiency.html> (accessed on 2 August 2020).
48. Seo, S.; Jeong, S.; Park, H.; Shin, H.; Park, N.-G. Atomic Layer Deposition for Efficient and Stable Perovskite Solar Cells. *Chem. Commun.* **2019**, *55*, 2403. [CrossRef] [PubMed]
49. Xu, X.; Liu, J.; Liu, J.; Ouyang, L.; Hu, R.; Wang, H.; Yang, L.; Zhu, M. A General Metal-Organic Framework (MOF)-Derived Selenidation Strategy for In Situ Carbon-Encapsulated Metal Selenides as High-Rate Anodes for Na-Ion Batteries. *Adv. Funct. Mater.* **2018**, *28*, 1707573. [CrossRef]
50. Javed, M.S.; Shah, H.U.; Shaheen, N.; Lin, R.; Qiu, M.; Xie, J.; Li, J.; Raza, R.; Mai, W.; Hu, C. High Energy Density Hybrid Supercapacitor Based on 3D Mesoporous Cuboidal Mn₂O₃ and MOF-Derived Porous Carbon Polyhedrons. *Electrochim. Acta* **2018**, *18*, 31296. [CrossRef]
51. Hou, A.X.; Pan, L.; Huang, S.; Ou-yang, W.; Chen, X. Enhanced Efficiency and Stability of Perovskite Solar Cells using Porous Hierarchical TiO₂ Nanostructures of Scattered Distribution as Scaffold. *Electrochim. Acta* **2017**, *17*, 30701.
52. Aubrey, M.L.; Wiers, B.M.; Andrews, S.C.; Sakurai, T.; Reyes-lillo, S.E.; Hamed, S.M.; Yu, C.; Darago, L.E.; Mason, J.A.; Baeg, J.; et al. Electron delocalization and Charge Mobility as a Function of Reduction in a Metal–Organic Framework. *Nat. Mater.* **2018**, *17*, 625. [CrossRef]
53. Vinogradov, A.V.; Zaake-hertling, H.; Hey-hawkins, E.; Agafonov, A.V.; Seisenbaeva, G.A.; Kessler, V.G.; Vinogradov, V.V. The first Depleted Heterojunction TiO₂–MOF-Based Solar Cell. *Chem. Commun.* **2014**, *1*, 14. [CrossRef]
54. Lee, C.; Chen, C.; Liao, Y.; Wu, K.C.; Chueh, C. Enhancing Efficiency and Stability of Photovoltaic Cells by Using Perovskite/Zr-MOF Heterojunction Including Bilayer and Hybrid Structures. *Adv. Sci.* **2018**, *6*, 1801715. [CrossRef]
55. Ryu, U.; Jee, S.; Park, J.; Han, I.K.; Lee, J.H.; Park, M.; Choi, K.M. Nanocrystalline Titanium Metal–Organic Frameworks for Highly Efficient and Flexible Perovskite Solar Cells. *ACS Nano* **2018**, *12*, 4968. [CrossRef] [PubMed]
56. My, T.; Nguyen, H.; Bark, C.W. Synthesis of Cobalt-Doped TiO₂ Based on Metal–Organic Frameworks as an Effective Electron Transport Material in Perovskite Solar Cells. *ACS Omega* **2020**, *5*, 2280.
57. Zhang, Y.; Li, B.; Fu, L.; Li, Q.; Yin, L. MOF-Derived ZnO as Electron Transport Layer for Improving Light Harvesting and Electron Extraction Efficiency in Perovskite Solar Cells. *Electrochim. Acta* **2019**, *330*, 135280. [CrossRef]
58. Li, M.; Wang, J.; Jiang, A.; Xia, D.; Du, X.; Dong, Y.; Wang, P.; Fan, R.; Yang, Y. Metal Organic Framework Doped Spiro-OMeTAD with Increased Conductivity for Improving Perovskite Solar Cell Performance. *Sol. Energy* **2019**, *188*, 380. [CrossRef]
59. Huang, L.; Zhou, X.; Wu, R.; Shi, C.; Xue, R.; Zou, J.; Xu, C.; Zhao, J.; Zeng, W. Oriented Haloing Metal-organic Framework Providing High Efficiency and High Moisture-Resistance for Perovskite Solar Cells, Journal of Power Sources. *J. Power Sources* **2019**, *433*, 226699. [CrossRef]
60. Zhou, X.; Qiu, L.; Fan, R.; Wang, A.; Ye, H.; Tian, C.; Hao, S.; Yang, Y. Metal–Organic Framework-Derived N-Rich Porous Carbon as an Auxiliary Additive of Hole Transport Layers for Highly Efficient and Long-Term Stable Perovskite Solar Cells. *RRL Sol.* **2019**, *4*, 1900380. [CrossRef]
61. Chang, T.; Kung, C.; Chen, H.; Huang, T.; Kao, S.; Lu, H.; Lee, M.; Boopathi, K.M.; Chu, C. Planar Heterojunction Perovskite Solar Cells Incorporating Metal–Organic Framework Nanocrystals. *Adv. Mater.* **2015**, *27*, 7229. [CrossRef]
62. Zhou, X.; Qiu, L.; Fan, R.; Zhang, J.; Hao, S.; Yang, Y. Heterojunction Incorporating Perovskite and Microporous Metal–Organic Framework Nanocrystals for Efficient and Stable Solar Cells. *Nano Micro Lett.* **2020**, *12*, 80. [CrossRef]
63. Abdulrazzaq, O.A.; Saini, V.; Bourdo, S.; Dervishi, E.; Biris, A.S. Organic Solar Cells: A Review of Materials, Limitations, and Possibilities for Improvement Omar. *Part Sci. Technol.* **2013**, *6351*, 427. [CrossRef]

64. Li, L.; Chang, Z.; Zhang, X. Recent Progress on the Development of Metal-Air Batteries, Advanced Sustainable Systems. *Adv. Sustain. Syst.* **2017**, *1*, 1700036. [CrossRef]
65. Zhang, J.; Zhou, Q.; Tang, Y.; Zhang, L.; Li, Y. Zinc–Air batteries: Are They Ready for Prime Time? *Chem. Sci.* **2019**, *10*, 8924. [CrossRef] [PubMed]
66. Nian, P.; Cao, Y.; Li, Y.; Zhang, X.; Wang, Y.; Liu, H.; Zhang, X. Reproduction of A Pure ZIF-67 Membrane by Self-Conversion of Cobalt Carbonate Hydroxide Nanowires for H₂ Separation. *Cryst. Eng. Comm.* **2018**, *20*, 2440. [CrossRef]
67. Imaz, I.; Cano-sarabia, M.; MasPOCH, D.; Carne, A. A Spray-Drying Strategy for Synthesis of Nanoscale Metal–Organic Frameworks and Their Assembly into Hollow Superstructures. *Nat. Chem.* **2013**, *5*, 203.
68. Simon-Yarza, T.; Gimenez-Marqués, M.; Mrimi, R.; Mielcarek, A.; Gref, R.; Horcajada, P.; Serre, C.; Couvreur, P. A Smart Metal-Organic-Framework Nanomaterial for Lung Targeting. *Angew. Chem. Int. Ed.* **2017**, *56*, 15565. [CrossRef]
69. Liu, W.; Yin, R.; Xu, X.; Zhang, L.; Shi, W.; Cao, X. Structural Engineering of Low-Dimensional Metal–Organic Frameworks: Synthesis, Properties, and Applications. *Adv. Sci.* **2019**, *6*, 1802373. [CrossRef]
70. Ji, H.; Wang, M.; Liu, S.; Sun, H.; Liu, J.; Qian, T.; Yan, C. Pyridinic and Graphitic Nitrogen-Enriched Carbon Paper as a Highly Active Bifunctional Catalyst for Zn-Air Batteries. *Electrochim. Acta* **2020**, *19*, 135562. [CrossRef]
71. Tian, G.; Zhao, M.; Yu, D.; Kong, X.; Huang, J. Nitrogen-Doped Graphene/Carbon Nanotube Hybrids: In Situ Formation on Bifunctional Catalysts and Their Superior Electrocatalytic Activity for Oxygen Evolution/Reduction Reaction. *Small* **2014**, *10*, 2251. [CrossRef]
72. Song, Z.; Han, X.; Deng, Y.; Zhao, N.; Hu, W.; Zhong, C. Clarifying the Controversial Catalytic Performance of Co(OH)₂ for Oxygen Reduction/Evolution Reactions Toward Efficient Zn-Air Batteries. *ACS Appl. Mater. Interfaces* **2017**, *9*, 22694. [CrossRef]
73. Zhu, B.; Liang, Z.; Xia, D.; Zou, R. Metal-Organic Frameworks and Their Derivatives for Metal-Air Batteries. *Energy Storage Mater.* **2019**, *23*, 2405. [CrossRef]
74. Anand, G. Technological Breakthrough Achieved for Recharging Zinc-Air Battery. *Trend Force*, 23 August 2017.
75. Tahil, W. The Zinc Air Battery and the Zinc Economy: A Virtuous Circle. *Meridian Int. Res.* **2007**, 1–9. Available online: http://www.meridian-int-res.com/Projects/The_Zinc_Air_Solution.pdf (accessed on 2 August 2020).
76. Cachet, C.; Saidani, B.; Wiart, R. The Behavior of Zinc Electrode in Alkaline Electrolytes: II. A Kinetic Analysis of Anodic Dissolution. *Electrochem. Soc.* **1992**, *139*, 644. [CrossRef]
77. Han, X.; Ling, X.; Wang, Y.; Ma, T.; Zhong, C.; Hu, W.; Deng, Y. Spatial Isolation of Zeolitic Imidazole Frameworks-Derived Cobalt Catalysts: From Nanoparticle, Atomic Cluster to Single Atom. *Angew. Chem.* **2019**, *131*, 5413. [CrossRef]
78. Liang, Z.; Guo, W.; Zhao, R.; Qiu, T.; Tabassum, H.; Zou, R. Engineering Atomically Dispersed Metal Sites for Electrocatalytic Energy Conversion. *Nano Energy* **2019**, *64*, 103917. [CrossRef]
79. Han, G.; Zheng, Y.; Zhang, X.; Wang, Z.; Gong, Y.; Du, C.; Norouzi, M.; Yiu, Y.; Sham, T.; Gu, L.; et al. High loading single-atom Cu Dispersed on Graphene for Efficient Oxygen Reduction Reaction. *Nano Energy* **2019**, *66*, 104088. [CrossRef]
80. Zhang, X.; Han, X.; Jiang, Z.; Xu, J.; Chen, L.; Xue, Y.; Nie, A.; Xie, Z.; Kuang, Q.; Zheng, L. Atomically Dispersed Hierarchically Ordered Porous Fe-N-C Electrocatalyst for High Performance Electrocatalytic Oxygen Reduction in Zn-Air Battery. *Nano Energy* **2020**, *71*, 104547. [CrossRef]
81. Lee, S.H.; Kim, J.; Chung, D.Y.; Yoo, J.M.; Lee, H.S.; Kim, M.J.; Mun, B.S.; Kwon, S.G.; Sung, Y.; Hyeon, T. Design Principle of Fe–N–C Electrocatalysts: How to Optimize Multimodal Porous Structures? *J. Am. Chem. Soc.* **2019**, *141*, 2035. [CrossRef]
82. Wang, X.; Chen, Z.; Zhao, X.; Yao, T.; Chen, W.; You, R.; Zhao, C.; Wu, G.; Wang, J.; Huang, W.; et al. Regulation of Coordination Number over Single Co Sites Triggers the Efficient Electroreduction of CO₂. *Angew. Chem. Int. Ed.* **2017**, *57*, 1944. [CrossRef]
83. Hai, X.; Zhao, X.; Guo, N.; Yao, C.; Chen, C.; Liu, W.; Yan, H.; Li, J.; Chen, Z.; Li, X.; et al. Engineering Local and Global Structure of Single Co Atom for Superior Oxygen Reduction Reaction. *ACS Catal.* **2020**, *10*, 5862. [CrossRef]
84. Wagh, N.K.; Shinde, S.S.; Lee, C.H.; Jung, J.; Kim, D.; Kim, S.; Lin, C.; Lee, S.U.; Lee, J. Densely Colonized Isolated Cu-N Single Sites for Efficient Bifunctional Electrocatalysts and Rechargeable Advanced Zn-Air Batteries. *Appl. Catal. B Environ.* **2020**, *268*, 118746. [CrossRef]

85. Wang, Z.; Ang, J.; Liu, J.; Yun, X.; Ma, D.; Kong, J.; Zhang, Y.; Yan, T.; Lu, X. FeNi alloys Encapsulated in N-doped CNTs-Tangled Porous Carbon Fibers as Highly Efficient and Durable Bifunctional Oxygen Electrocatalyst for Rechargeable Zinc-Air Battery. *Appl. Catal. B Environ.* **2019**, *19*, 118344.
86. Agarwal, S.; Yu, X.; Manthiram, A. A Pair of Metal Organic Framework (MOF) -Derived Oxygen Reduction Reaction (ORR) and Oxygen Evolution Reaction (OER) Catalysts for Zinc-Air Batteries. *Mater. Today Energy* **2020**, *16*, 100405. [[CrossRef](#)]
87. Wu, M.; Zhang, G.; Qiao, J.; Chen, N.; Chen, W.; Sun, S.; National, I.; Recherche, D.; Matériaux, S.-E. Ultra-Long Life Rechargeable Zinc-Air Battery Based on High-Performance Trimetallic Nitride and NCNT Hybrid Bifunctional Electrocatalysts. *Nano Energy* **2019**, *61*, 86. [[CrossRef](#)]
88. Zhang, J.; Zhang, M.; Zeng, Y.; Chen, J.; Qiu, L.; Zhou, H.; Sun, C. Single Fe Atom on Hierarchically Porous S, N-Codoped Nanocarbon Derived from Porphyrin Enable Boosted Oxygen Catalysis for Rechargeable Zn-Air Batteries. *Small* **2019**, *15*, 1900307. [[CrossRef](#)] [[PubMed](#)]
89. Guo, D.; Shibuya, R.; Akiba, C.; Saji, S.; Kondo, T.; Nakamura, J. Active Sites of Nitrogen-Doped Carbon Materials for Oxygen Reduction Reaction Clarified using Model Catalysts. *Science* **2016**, *351*, 361. [[CrossRef](#)]
90. Sarkar, S.; Biswas, A.; Purkait, T.; Das, M.; Kamboj, N.; Dey, R.S. Unravelling the Role of Fe–Mn Binary Active Sites Electrocatalyst for Efficient Oxygen Reduction Reaction and Rechargeable Zn-Air Batteries. *Inorg. Chem.* **2020**, *59*, 5194. [[CrossRef](#)]
91. Najam, T.; Shoaib, S.; Shah, A.; Ali, H.; Song, Z.; Sun, H.; Peng, Z.; Cai, X. A Metal Free Electrocatalyst for High-Performance Zinc-Air Battery Application with Good Resistance towards Poisoning Species. *Carbon* **2020**, *164*, 12. [[CrossRef](#)]
92. Wang, D.; Su, D. Heterogeneous Nanocarbon Materials for Oxygen Reduction Reaction. *Energy Environ. Sci.* **2014**, *7*, 576. [[CrossRef](#)]
93. Maciel, I.O.; Pimenta, M.A.; Sumpter, B.G.; Meunier, V.; Lo, F. Synthesis, Electronic Structure, and Raman Scattering of Phosphorus-Doped Single-Wall Carbon Nanotubes. *Nano Lett.* **2008**, *9*, 2267. [[CrossRef](#)]
94. Zhang, J.; Dai, L. Electrochemical Water Splitting Hot Paper Nitrogen, Phosphorus, and Fluorine Tri-doped Graphene as a Multifunctional Catalyst for Self-Powered Electrochemical Water Splitting. *Angew. Chem. Int. Ed.* **2016**, *55*, 1. [[CrossRef](#)]
95. He, B.; Liu, F.; Yan, S. Temperature-Direct Growth of Graphitized, Ultra-hollow Carbon Framework of Highly Pyridinic Nitrogen Doped as an Efficient Electrocatalyst for Oxygen Reduction Reaction. *J. Mater. Chem. A* **2017**, *5*, 18064. [[CrossRef](#)]
96. Zhang, J.; Dai, L. Heteroatom-Doped Graphitic Carbon Catalysts For Efficient Electrocatalysis Of Oxygen Reduction Reaction. *ACS Catal.* **2015**, *5*, 7244. [[CrossRef](#)]
97. Xing, Y.; Chen, N.; Luo, M.; Sun, Y.; Yang, Y.; Qian, J.; Li, L. Long-life Lithium-O₂ Battery Achieved by Integrating Quasi-Solid Electrolyte and Highly Active Pt₃Co Nanowires Catalyst. *Energy Storage Mater.* **2019**, *24*, 707. [[CrossRef](#)]
98. Abraham, K.M.; Jiang, Z. A Polymer Electrolyte-Based Rechargeable lithium/Oxygen Battery. *J. Electrochem. Soc.* **1996**, *143*, 1. [[CrossRef](#)]
99. Wu, F.; Yu, Y. Toward True Lithium-Air Batteries. *Joule* **2018**, *2*, 815. [[CrossRef](#)]
100. Wang, Y.; Zhou, H. A Lithium-Air Battery with A Potential to Continuously Reduce O₂ from Air for Delivering Energy. *J. Power Sources* **2010**, *195*, 358. [[CrossRef](#)]
101. Lai, N.; Cong, G.; Liang, Z.; Lu, Y.; Lai, N.; Cong, G.; Liang, Z.; Lu, Y. A Highly Active Oxygen Evolution Catalyst for Lithium-Oxygen Batteries Enabled by High- Surface-Energy Facets. *Joule* **2018**, *2*, 1. [[CrossRef](#)]
102. Wang, Y.; Lai, N.; Lu, Y.; Zhou, Y.; Dong, C.; Lu, Y.; Wang, Y.; Lai, N.; Lu, Y.; Zhou, Y.; et al. A Solvent-Controlled Oxidation Mechanism of Li₂O₂ in Lithium-Oxygen Batteries. *Joule* **2017**, *2*, 1. [[CrossRef](#)]
103. Jin, C.; Yang, Z.; Cao, X.; Lu, F.; Yang, R. A Novel Bifunctional Catalyst of Ba_{0.9}Co_{0.5}Fe_{0.4}Nb_{0.1}O₃Ld Perovskite for Lithium-Air Battery. *Int. J. Hydrogen Energy* **2013**, *39*, 2526. [[CrossRef](#)]
104. Geng, D.; Ding, N.; Hor, T.S.A.; Chien, S.W.; Liu, Z. Rom Lithium-Oxygen to Lithium-Air Batteries: Challenges and Opportunities. *Adv. Energy Mater.* **2016**, *6*, 1502164. [[CrossRef](#)]
105. Lyu, Z.; Lim, G.J.H.; Guo, R.; Kou, Z.; Wang, T.; Guan, C.; Ding, J.; Chen, W.; Wang, J. 3D-Printed MOF-Derived Hierarchically Porous Frameworks for Practical High-Energy Density Li–O₂ Batteries. *Adv. Funct. Mater.* **2018**, *29*, 1806658. [[CrossRef](#)]

106. Meng, X.; Liao, K.; Dai, J.; Zou, X.; She, S.; Zhou, W.; Ye, F.; Shao, Z. Ultralong Cycle Life Li–O₂ Battery Enabled by a MOF-Derived Ruthenium–Carbon Composite Catalyst with a Durable Regenerative Surface. *ACS Appl. Mater. Interfaces* **2019**, *11*, 20091. [[CrossRef](#)] [[PubMed](#)]
107. Liu, Y.; Jiang, H.; Zhu, Y.; Yang, X.; Li, C. Transitional Metal (Fe, Co, Ni) Encapsulated in Nitrogen-Doped Carbon Nanotubes as Bi-functional Catalysts for Oxygen Electrode Reactions. *J. Mater. Chem. A* **2016**, *4*, 1694. [[CrossRef](#)]
108. Wang, X.; Zhang, F.; Liu, Y.; Wang, Z. Nitrogen-Doped Carbon Nanotubes Encapsulated Cobalt Nanoparticles Hybrids for Highly Efficient Catalysis of Oxygen Reduction Reaction. *J. Electrochem. Soc.* **2018**, *165*, 3052. [[CrossRef](#)]
109. Wang, X.; Zhang, H.; Lin, H.; Gupta, S.; Wang, C.; Tao, Z.; Fu, H.; Wang, T.; Zheng, J.; Wu, G.; et al. Nano Energy Directly Converting Fe-doped Metal–Organic Frameworks into Highly Active and Stable Fe–N–C Catalysts for Oxygen Reduction in Acid. *Nano Energy* **2016**, *25*, 110. [[CrossRef](#)]
110. Khalid, M.; Honorato, A.M.B.; Dai, L. Multifunctional Electrocatalysts Derived from Conducting Polymer and Metal Organic Framework Complexes. *Nano Energy* **2017**, *17*, 30819. [[CrossRef](#)]
111. Hou, Y.; Hou, C.; Zhai, Y.; Li, H.; Chen, T.; Fan, Y.; Wang, H.; Wang, W. Enhancing the Electrocatalytic Activity of 2D Micro-Assembly Co₃O₄ Nanosheets for Li–O₂ Batteries by Tuning Oxygen Vacancies and Co³⁺/Co²⁺ ratio. *Electrochim. Acta* **2019**, *324*, 134884. [[CrossRef](#)]
112. Ma, F.; Wu, H.B.; Xia, B.Y.; Xu, C.; Wen, X.; Lou, D. Hierarchical Beta-Mo₂C Nanotubes Organized by Ultrathin Nanosheets as a Highly Efficient Electrocatalyst for Hydrogen Production. *Angew. Chem.* **2015**, *54*, 15395. [[CrossRef](#)]
113. Jong, Y.; Hyun, J.; Park, S.; Park, J.; Lee, J.; Chan, Y. Highly Efficient Hierarchical Multiroom-Structured Molybdenum Carbide/ Carbon Composite Microspheres Grafted with Nickel-Nanoparticle-Embedded Nitrogen-Doped Carbon Nanotubes as Air Electrode for Lithium–Oxygen Batteries. *Chem. Eng. J.* **2018**, *351*, 886.
114. Kelly, T.G.; Lee, K.X.; Chen, J.G. Pt-Modified Molybdenum Carbide for the Hydrogen Evolution Reaction: From Model Surfaces to Powder Electrocatalysts. *J. Power Sources* **2014**, *271*, 76. [[CrossRef](#)]
115. Oh, Y.J.; Kim, J.H.; Lee, J.Y.; Park, S.-K.; Kang, Y.C. Design of House Centipede-like MoC–Mo₂C Nanorods Grafted with N-Doped Carbon Nanotubes as Bifunctional Catalysts for High-Performance Li–O₂ Batteries. *Chem. Eng. J.* **2019**, *19*, 32757. [[CrossRef](#)]
116. Zhang, M.; Dai, Q.; Zheng, H.; Chen, M.; Dai, L. Novel MOF-Derived Co@N–C Bifunctional Catalysts for Highly Efficient Zn–Air Batteries and Water Splitting. *Adv. Mater.* **2018**, *1705431*, 1. [[CrossRef](#)] [[PubMed](#)]
117. Li, S.; Dong, Y.; Zhou, J.; Liu, Y.; Wang, J.; Gao, X.; Han, Y.; Qi, P.; Wang, B. Carbon Dioxide in the Cage: Manganese Metal–Organic Frameworks for High Performance CO₂ Electrodes in Li–CO₂ Batteries. *Energy Environ. Sci.* **2018**, *11*, 1318. [[CrossRef](#)]
118. Chao, F.; Wang, B.; Ren, J.; Lu, Y.; Zhang, W.; Wang, X.; Cheng, L.; Lou, Y.; Chen, J. Micro–Meso–Macroporous FeCo–N–C Derived from Hierarchical Bimetallic FeCo–ZIFs as Cathode Catalysts for Enhanced Li–O₂ Batteries Performance. *J. Energy Chem.* **2019**, *35*, 212. [[CrossRef](#)]
119. Li, J.; Deng, Y.; Leng, L.; Liu, M.; Huang, L.; Tian, X.; Song, H.; Lu, X. MOF-Templated Sword-Like Co₃O₄@NiCo₂O₄ Sheet Arrays on Carbon Cloth as Highly Efficient Li–O₂ Battery Cathode. *J. Power Sources* **2020**, *450*, 227725. [[CrossRef](#)]
120. Hu, X.; Cheng, F.; Zhang, N.; Han, X.; Chen, J. Nanocomposite of Fe₂O₃@C@MnO₂ as an Efficient Cathode Catalyst for Rechargeable Lithium–Oxygen Batteries. *Small* **2015**, *2*, 5545. [[CrossRef](#)]
121. Zhang, X.; Dong, P.; Lee, J.; Jake, T.; Cha, Y.; Ha, S.; Song, M. Enhanced Cycling Performance of Rechargeable Li–O₂ Batteries via LiOH Formation and Decomposition Using High-Performance MOF-74@CNTs Hybrid Catalysts. *Energy Storage Mater.* **2018**, *18*, 30801. [[CrossRef](#)]
122. Wang, H.; Yin, F.; Liu, N.; Kou, R.; He, X.; Sun, C.; Chen, B.; Liu, D.; Yin, H. Engineering Fe–Fe₃C@Fe–N–C Active Sites and Hybrid Structures from Dual Metal–Organic Frameworks for Oxygen Reduction Reaction in H₂–O₂ Fuel Cell and Li–O₂ Battery. *Adv. Funct. Mater.* **2019**, *29*, 1901531. [[CrossRef](#)]
123. Chatterjee, A.; Or, S.W. Metal–Organic Framework-Derived MnO/CoMn₂O₄@N–C nanorods with Nanoparticle Interstitial Decoration in Core@Shell Structure as Improved Bifunctional Electrocatalytic Cathodes for Li–O₂ Batteries. *Electrochim. Acta* **2020**, *20*, 135809. [[CrossRef](#)]

124. Liang, R.; Hu, A.; Li, M.; Ran, Z.; Shu, C.; Long, J. Cobalt Encapsulated within Porous MOF-Derived Nitrogen-Doped Carbon as an Efficient Bifunctional Electrocatalyst for Aprotic Lithium-Oxygen Battery. *J. Alloys Compd.* **2019**, *810*, 151877. [[CrossRef](#)]
125. Yu, S.; Luo, S.; Zhan, Y.; Huang, H.; Wang, Q. Metal-Organic Framework-Derived Cobalt Nanoparticle Space Confined in Nitrogen-Doped Carbon Polyhedra Networks as High-Performance Bifunctional Electrocatalyst for Rechargeable Li–O₂ Batteries. *J. Power Sources* **2020**, *453*, 227899. [[CrossRef](#)]
126. Zhao, Y.; Song, Z.; Li, X.; Sun, Q.; Cheng, N.; Lawes, S.; Sun, X. Metal Organic Frameworks for Energy Storage and Conversion. *Energy Storage Mater.* **2015**, *15*, 30056. [[CrossRef](#)]
127. Egan, D.R.; de León, C.P.; Wood, R.J.K.; Jones, R.L.; Stokes, K.R.; Walsh, F.C. Developments in Electrode Materials and Electrolytes for Aluminum–Air Batteries. *J. Power Sources* **2013**, *236*, 293. [[CrossRef](#)]
128. Li, Q.; Bjerrum, N.J. Aluminum as Anode for Energy Storage and Conversion: A Review. *J. Power Sources* **2002**, *110*, 1. [[CrossRef](#)]
129. Hang, C.; Zhang, J.; Zhu, J.; Li, W.; Kou, Z.; Huang, Y. In Situ Exfoliating and Generating Active Sites on Graphene Nanosheets Strongly Coupled with Carbon Fiber toward Self-Standing Bifunctional Cathode for Rechargeable Zn–Air Batteries. *Adv. Energy Mater.* **2018**, *8*, 1703539. [[CrossRef](#)]
130. Xu, J.; Chang, Z.; Wang, Y.; Liu, D.; Zhang, Y.; Zhang, X. Metal–Air Batteries with High Energy Density: Li–Air versus Zn–Air. *Adv. Mater.* **2016**, *28*, 9620. [[CrossRef](#)]
131. Mori, R. Electrochemical Properties of A Rechargeable Aluminum–Air Battery with A Metal–Organic Framework as Air Cathode Material. *RSC Adv.* **2017**, *7*, 6389. [[CrossRef](#)]
132. Abdel-Gaber, A.M.; Khamis, E.; Adeel, S. Novel Package for Inhibition of Aluminium Corrosion in Alkaline Solutions. *Mater. Chem. Phys.* **2010**, *124*, 773. [[CrossRef](#)]
133. Flamini, D.O.; Saidman, S.B.; Bessone, J.B. Aluminum Activation Produced by Gallium. *Corros. Sci.* **2006**, *48*, 1413. [[CrossRef](#)]
134. Bessone, J.B.; Flamini, D.O.; Saidman, S.B. Comprehensive Model for the Activation Mechanism of Al–Zn Alloys Produced by Indium. *Corros. Sci.* **2005**, *47*, 95. [[CrossRef](#)]
135. Zhang, Z.; Zuo, C.; Liu, Z.; Yu, Y.; Zuo, Y.; Song, Y. All-Solid-State Al e Air Batteries with Polymer Alkaline Gel Electrolyte. *J. Power Sources* **2014**, *251*, 470. [[CrossRef](#)]
136. Nestoridi, M.; Pletcher, D.; Wood, R.J.K.; Wang, S.; Jones, R.L.; Stokes, K.R.; Wilcock, I. The Study of Aluminium Anodes for High Power Density Al/Air Batteries with Brine Electrolytes. *J. Power Sources* **2008**, *178*, 445. [[CrossRef](#)]
137. Xu, Y.; Zhao, Y.; Ren, J.; Zhang, Y.; Peng, H. An All-Solid-State Fiber-Shaped Aluminum–Air Battery with Flexibility, Stretchability, and High Electrochemical Performance. *Angew. Chem.* **2016**, *128*, 1. [[CrossRef](#)]
138. Zhang, T.; Li, Z.; Zhang, Z.; Wang, L.; Sun, P.; Wang, S. Design of Three Dimensional Interconnected Hierarchical Micro- Mesoporous Structure of Graphene as Support Material for Spinel NiCoO Electrocatalyst toward Oxygen Reduction Reaction. *J. Phys. Chem. C* **2018**, *48*, 27469. [[CrossRef](#)]
139. Wang, C.; Li, Z.; Wang, L.; Lu, X.; Wang, S.; Niu, X. Vertical-Space-Limit Synthesis of Bi-Functional Fe, N codoped Two- Dimensional Multilayers Graphene Electrocatalysts for Zn-air Battery. *Energy Technol.* **2019**, *7*, 1900123. [[CrossRef](#)]
140. Jiang, M.; Yang, J.; Ju, J.; Zhang, W.; He, L.; Zhang, J.; Fu, C.; Sun, B. Pace-Confined Synthesis of CoNi nanoalloy in N-doped Porous Carbon Frameworks as Efficient Oxygen Reduction Catalyst for Neutral and Alkaline Aluminum-air Batteries. *Energy Storage Mater.* **2020**, *20*, 30022.
141. Liu, Y.; Jiang, H.; Hao, J.; Liu, Y.; Shen, H.; Li, W.; Li, J. Metal-Organic Framework Derived Reduced Graphene Oxide Supported ZnO/ZnCo₂O₄/C Hollow Nanocages as Cathode Catalysts for Aluminum-O₂ Batteries. *ACS Appl. Mater. Interfaces* **2017**, *9*, 31841. [[CrossRef](#)]
142. Li, J.; Zhou, N.; Song, J.; Fu, L.; Yan, J.; Tang, Y.; Wang, H. Cu-MOF-Derived Cu/Cu₂O Nanoparticles and Cu_NxCy Species to Boost Oxygen Reduction Activity of Ketjenblack Carbon in Al-Air Battery. *ACS Sustain. Chem. Eng.* **2018**, *6*, 413. [[CrossRef](#)]
143. Wang, J.; Lu, H.; Hong, Q.; Cao, Y.; Li, X.; Bai, J. Porous N,S-Codoped Carbon Architectures with Bimetallic Sulphide Nanoparticles Encapsulated in Graphitic Layers: Highly Active and Robust Electrocatalysts for the Oxygen Reduction Reaction in Al-Air Batteries. *Chem. Eng. J.* **2017**, *17*, 31415. [[CrossRef](#)]
144. Lou, P.; Li, C.; Cui, Z.; Guo, X. Job-Sharing Cathode Design for Li–O₂ Batteries with High Energy Efficiency Enabled by In-Situ Ionic Liquid Bonding to Cover Carbon Surface Defects. *J. Mater. Chem. A* **2015**, *8*, 1703539.

145. Zhang, S.S.; Foster, D.; Read, J. Discharge Characteristic of A Non-Aqueous Electrolyte Li/O₂ Battery. *J. Power Sources* **2010**, *195*, 1235. [[CrossRef](#)]
146. Wei, S.; Xu, S.; Agrawal, A.; Choudhury, S.; Lu, Y.; Tu, Z.; Ma, L.; Archer, L.A. A Stable Room-Temperature Sodium–Sulfur Battery. *Nat. Commun.* **2016**, *7*, 1. [[CrossRef](#)] [[PubMed](#)]
147. Choudhury, S.; Wei, S.; Ozhabes, Y.; Gunceler, D.; Zachman, M.J.; Tu, Z.; Shin, J.H.; Nath, P.; Agrawal, A.; Kourkoutis, L.F.; et al. Designing Solid-Liquid Interphases for Sodium Batteries. *Nat. Commun.* **2017**, *8*, 898. [[CrossRef](#)] [[PubMed](#)]
148. Lu, X.; Xia, G.; Lemmon, J.P.; Yang, Z. Advanced Materials for Sodium-Beta Alumina Batteries: Status, Challenges and Perspectives. *J. Power Sources* **2010**, *195*, 2431. [[CrossRef](#)]
149. Kim, S.; Seo, D.; Ma, X.; Ceder, G.; Kang, K. Electrode Materials for Rechargeable Sodium-Ion Batteries: Potential Alternatives to Current Lithium-Ion Batteries. *Adv. Energy Mater.* **2012**, *2*, 710. [[CrossRef](#)]
150. Kim, M.; Ju, H.; Kim, J. Highly Efficient Bifunctional Catalytic Activity of Bismuth Rhodium Oxide Pyrochlore Through Tuning the Covalent Character for Rechargeable Aqueous Na-Air Batteries. *J. Mater. Chem. A* **2018**, *6*, 8523. [[CrossRef](#)]
151. Peled, E.; Golodnitsky, D.; Mazor, H.; Goor, M.; Avshalomov, S. Parameter Analysis of A Practical Lithium- and Sodium-Air Electric Vehicle Battery. *J. Power Sources* **2011**, *196*, 6835. [[CrossRef](#)]
152. Khan, Z.; Vagin, M.; Crispin, X. Can Hybrid Na–Air Batteries Outperform Nonaqueous Na–O₂ Batteries? *Adv. Sci.* **2020**, *7*, 1902866. [[CrossRef](#)]
153. Kim, J.; Lim, H.; Gwon, H.; Kang, K. Sodium–Oxygen Batteries with Alkyl-Carbonate and Ether Based Electrolytes. *Phys. Chem. Chem. Phys.* **2013**, *15*, 3623. [[CrossRef](#)]
154. Suntivich, J.; Gasteiger, H.A.; Yabuuchi, N.; Nakanishi, H.; Goodenough, J.B.; Shao-horn, Y. Design Principles for Oxygen-Reduction Activity on Perovskite Oxide Catalysts for Fuel Cells and Metal–Air Batteries. *Nat. Chem.* **2011**, *3*, 546. [[CrossRef](#)]
155. Suntivich, J.; May, K.J.; Gasteiger, H.A.; Goodenough, J.B.; Shao-Horn, Y. A Perovskite Oxide Optimized for Oxygen Evolution Catalysis from Molecular Orbital Principles. *Science* **2012**, *1383*, 1383–1385. [[CrossRef](#)]
156. Zhang, J.; Zhao, Z.; Xia, Z.; Dai, L. A Metal-Free Bifunctional Electrocatalyst for Oxygen Reduction and Oxygen Evolution Reactions. *Nat. Nanotechnol.* **2015**, *10*, 444. [[CrossRef](#)] [[PubMed](#)]
157. Chen, Q.; Hou, C.; Wang, C.; Yang, X.; Chen, Y. Ir⁴⁺-Doped NiFe LDH to Expedite Hydrogen Evolution Kinetics as A Pt-Like Electrocatalyst for Water Splitting. *Chem. Commun.* **2018**, *54*, 6400. [[CrossRef](#)] [[PubMed](#)]
158. Wang, Y.J.; Fang, B.; Zhang, D.; Li, A.; Wilkinson, D.P.; Ignaszak, A.; Zhang, L. A Review of Carbon-Composited Materials as Air-Electrode Bifunctional Electrocatalysts for Metal–Air Batteries. *Electrochem. Energy Rev.* **2018**, *1*, 1. [[CrossRef](#)]
159. Zhu, J.; Qu, T.; Su, F.; Wu, Y.; Kang, Y.; Chen, K.; Yao, Y.; Ma, W.; Yang, B.; Dai, Y.; et al. Highly dispersed Co Nanoparticles Decorated on N-doped Defective Carbon Nano-Framework for Hybrid Na-Air battery. *Dalton Trans.* **2020**, *49*, 1811. [[CrossRef](#)] [[PubMed](#)]
160. Liu, Y.; Xiaowei, L.; Qi, C.; Yuexiu, H.; Jiaqi, D.; Xinghao, H.; Yu, L. Metal-Organic Framework-Derived Hierarchical Co₃O₄@MnCo₂O_{4.5} Nanocubes with Enhanced Electrocatalytic Activity for Na-O₂ Batteries. *Nanoscale* **2019**, *11*, 5285. [[CrossRef](#)] [[PubMed](#)]

